

Fully integrated silicon probes for high-density recording of neural activity

James J. Jun^{1*}, Nicholas A. Steinmetz^{2,3,4*}, Joshua H. Siegle^{5*}, Daniel J. Denman^{5*}, Marius Bauza^{6,7*}, Brian Barbarits^{1*}, Albert K. Lee^{1*}, Costas A. Anastassiou^{5,8}, Alexandru Andrei⁹, Çağatay Aydın^{10,11}, Mladen Barbic¹, Timothy J. Blanche^{5,12}, Vincent Bonin^{9,10,11,13}, João Couto^{10,11}, Barundeb Dutta⁹, Sergey L. Gratiy⁵, Diego A. Gutnisky¹, Michael Häusser^{3,14}, Bill Karsh¹, Peter Ledochowitsch⁵, Carolina Mora Lopez⁹, Catalin Mitelut^{5,8}, Silke Musa⁹, Michael Okun^{2,3,15}, Marius Pachitariu^{2,3}, Jan Putzeys⁹, P. Dylan Rich¹, Cyrille Rossant^{2,3}, Wei-lung Sun¹, Karel Svoboda¹, Matteo Carandini⁴, Kenneth D. Harris^{2,3}, Christof Koch⁵, John O'Keefe^{6,7} & Timothy D. Harris¹

Sensory, motor and cognitive operations involve the coordinated action of large neuronal populations across multiple brain regions in both superficial and deep structures^{1,2}. Existing extracellular probes record neural activity with excellent spatial and temporal (sub-millisecond) resolution, but from only a few dozen neurons per shank. Optical Ca²⁺ imaging^{3–5} offers more coverage but lacks the temporal resolution needed to distinguish individual spikes reliably and does not measure local field potentials. Until now, no technology compatible with use in unrestrained animals has combined high spatiotemporal resolution with large volume coverage. Here we design, fabricate and test a new silicon probe known as Neuropixels to meet this need. Each probe has 384 recording channels that can programmably address 960 complementary metal–oxide–semiconductor (CMOS) processing-compatible low-impedance TiN⁶ sites that tile a single 10-mm long, 70 × 20-μm cross-section shank. The 6 × 9-mm probe base is fabricated with the shank on a single chip. Voltage signals are filtered, amplified, multiplexed and digitized on the base, allowing the direct transmission of noise-free digital data from the probe. The combination of dense recording sites and high channel count yielded well-isolated spiking activity from hundreds of neurons per probe implanted in mice and rats. Using two probes, more than 700 well-isolated single neurons were recorded simultaneously from five brain structures in an awake mouse. The fully integrated functionality and small size of Neuropixels probes allowed large populations of neurons from several brain structures to be recorded in freely moving animals. This combination of high-performance electrode technology and scalable chip fabrication methods opens a path towards recording of brain-wide neural activity during behaviour.

Historically, the most widely used tool for recording neuronal activity has been the extracellular microelectrode⁷. To make further progress in understanding the coordinated activity underlying brain computations, it is crucial to increase the number of single neurons that can be simultaneously monitored^{8–10}. This requires large dense arrays of recording sites, ideally compatible with freely moving rodents. To this end, we designed, fabricated and tested a new class of silicon probes¹¹.

Neuropixels probes were developed in three phases (see Supplementary Information) with seven design goals. The first two goals were: (1) dense and extensive recording sites to isolate individual neurons across large regions of the brain¹², and (2) a small cross-sectional area to minimize brain tissue damage. We achieved these two

goals using a custom 130-nm CMOS fabrication process¹³. This process allowed us to place 960 sites on a single, 10-mm long, non-tapered shank with 70 × 20-μm cross-section. This site count on a single shank is a large improvement over existing multi-shank silicon probes^{14–16}. We chose to focus on maximizing site count and minimizing width for a single shank because it presented the most essential engineering challenges. The solutions can be extended in a straightforward manner to multiple shanks for transverse coverage. The 12 × 12-μm sites are arranged in a checkerboard pattern with 4 columns and 25-μm

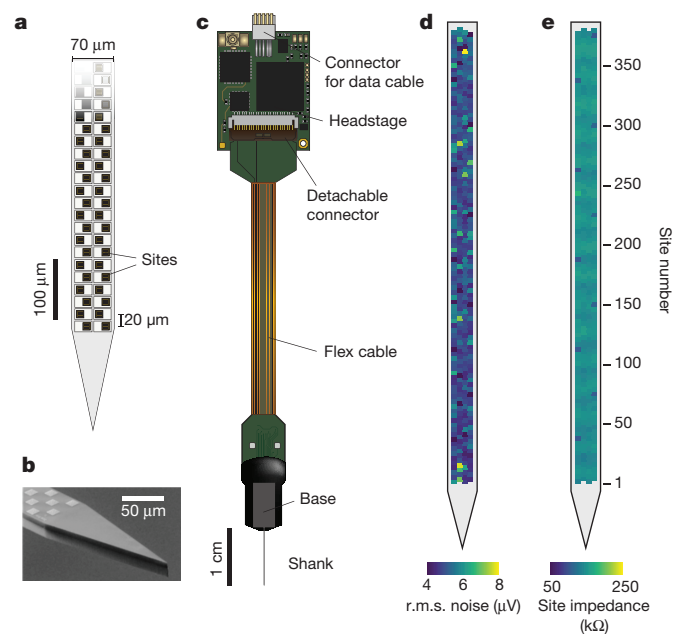


Figure 1 | The Neuropixels probe. **a**, Illustration of probe tip, showing checkerboard site layout (dark squares). **b**, Scanning electron microscope image of probe tip. **c**, Probe packaging, including flex cable and headstage for bidirectional data transmission. **d**, Example of r.m.s. noise levels of the AP band in saline, for 384 sites (switchable option). Mean \pm s.d. = $5.1 \pm 0.6 \mu\text{V}$. **e**, Typical site impedance in saline, for 384 sites, measured for each site with sinusoidal 1 nA injected currents at 1 kHz (see Methods). Mean \pm s.d. = $149 \pm 6 \text{ k}\Omega$.

¹HMMI Janelia Research Campus, 19700 Helix Drive, Ashburn, Virginia 20147, USA. ²UCL Institute of Neurology, University College London, London WC1N 3BG, UK. ³Department of Neuroscience, Physiology and Pharmacology, University College London, London WC1E 6DE, UK. ⁴UCL Institute of Ophthalmology, University College London, London EC1V 9EL, UK. ⁵Allen Institute for Brain Science, 615 Westlake Avenue North, Seattle, Washington 98109, USA. ⁶Department of Cell and Developmental Biology, University College London, London WC1E 6BT, UK. ⁷Sainsbury Wellcome Centre, University College London, London W1T 4JG, UK. ⁸Department of Neurology, University of British Columbia, Vancouver, British Columbia V6T 2B5, Canada. ⁹imec, Kapeldreef 75, 3001 Heverlee, Leuven, Belgium. ¹⁰Neuro-Electronics Research Flanders, Kapeldreef 75, 3001 Leuven, Belgium. ¹¹KU Leuven, Department of Biology, Naamsestraat 59, 3000 Leuven, Belgium. ¹²White Matter LLC, 999 3rd Avenue 700, 98104 Seattle, USA. ¹³VIB, 3001 Leuven, Belgium. ¹⁴Wolfson Institute for Biomedical Research, University College London, Gower Street, London WC1E 6BT, UK. ¹⁵Centre for Systems Neuroscience, University of Leicester, Leicester LE1 7QR, UK.

*These authors contributed equally to this work.

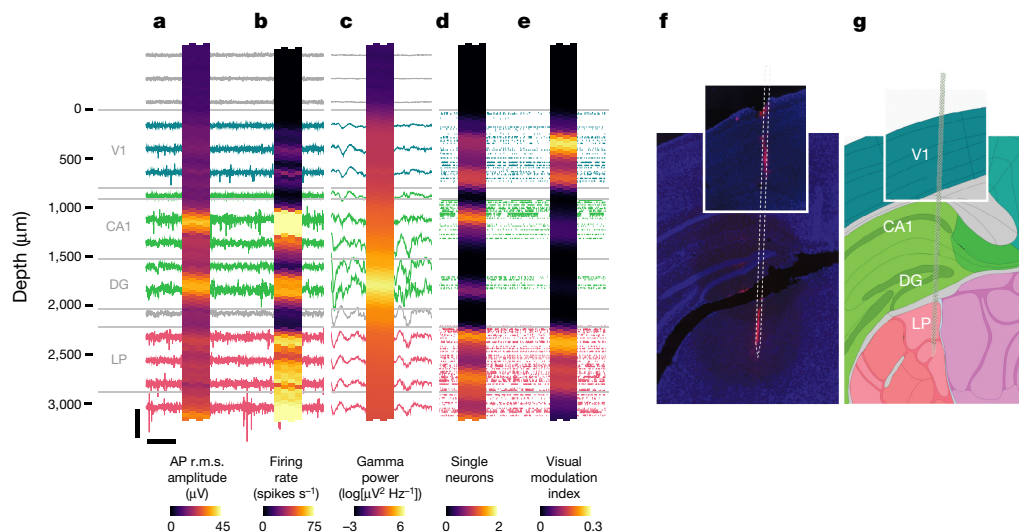


Figure 2 | Recording from large neuronal populations with a single probe in an awake head-fixed mouse. Signals were acquired from a Neuropixels probe inserted through primary visual cortex (V1), CA1 and dentate gyrus (DG) regions of the hippocampus, and the lateral posterior (LP) nucleus of the thalamus. Approximate structure boundaries are shown in grey next to the probe depth scale. For the heat maps, each square represents a single site. **a**, r.m.s. amplitude of the AP band signal for 1-s intervals, averaged over 10 intervals. **b**, Firing rate measured from AP band crossings of a $-50\mu\text{V}$ threshold, in a 10-s interval. **c**, Gamma-band LFP power (35–80 Hz), computed by Welch's method in a 1-s interval, averaged over 10 intervals. **d**, Distribution of putative single neuron locations (channel with peak amplitude), smoothed with a one-dimensional Gaussian filter (radius = 4.5 sites). **e**, Visual modulation index of spike activity (defined as $((x - y)/x)^2$, in which x is

the seventy-fifth percentile of the peristimulus time histogram and y is the twenty-fifth percentile) in response to 20-Hz visual flicker (15-s duration), for single neurons closest to each recording site, smoothed with a one-dimensional Gaussian filter (radius = 6 sites). Behind the heat maps are example traces from every twenty-fifth channel shown for the AP band (behind panels **a** and **b**) and the LFP band (behind panel **c**), along with example spike rasters for all putatively isolated single neurons (behind panel **d** and **e**, during visual flicker stimulation); $n = 103$ neurons in the thalamus, 41 in the hippocampus, and 62 in the cortex. Vertical/horizontal scale bars: AP band (**a**, **b**), $315\mu\text{V}/165\text{ms}$; LFP band (**c**), $1,550\mu\text{V}/290\text{ms}$; single neuron (**d**, **e**), 2.6 s. **f**, Histological reconstruction of the probe track with 4',6-diamidino-2-phenylindole (DAPI; blue) and DiI (red) staining. **g**, Corresponding images 81 and 82 from the Allen Mouse Brain Atlas.

centre-to-centre nearest neighbour spacing (Fig. 1a, b). Neuropixels probes feature user-programmable switches that allow the recording channels to address 384 of the 960 total sites simultaneously. We found no performance loss for switchable sites compared to a test version of the probe with unswitchable sites (Extended Data Fig. 1a, b).

We further sought to develop probes with (3) low noise, (4) resistance to movement artefacts or other interference, and (5) efficient data transmission by integrating low noise analogue amplifiers, multiplexers and digitizers into the probe base. This integration enables small size, minimal weight, noise immunity, and a digital data output stream transmitted via a single thin cable. The $6 \times 9\text{-mm}$ base, fabricated with the same CMOS processes used for the shank, yielded a finished probe of approximately 250 mg in weight, small enough for chronic implants in mice (Fig. 1c). We used 10-bit analogue-to-digital converters to minimize the base area and power consumption. Because 10 bits do not provide sufficient resolution for wideband recording, the continuous data stream from each channel was split into action potential (AP, 0.3–10 kHz) and local field potential (LFP, 0.5–1,000 Hz) bands that were separately amplified and digitized (AP, 30 kHz; LFP, 2.5 kHz). Together with low impedance TiN sites (see later) this system achieves uniform low noise (AP band $\sim 5\mu\text{V}$ root-mean squared (r.m.s.)) Fig. 1d; LFP band $\sim 9\mu\text{V}$ r.m.s.; Extended Data Table 1, options 1 and 3). We explored the use of on-site amplifiers (buffer amplifiers under each site) but found no advantage in performance (Extended Data Figs 1c–f and 2). Furthermore, such active probes had increased noise (Extended Data Table 1) and light sensitivity (Extended Data Fig. 3a, b).

Finally, we sought to (6) enable long-term recording stability and (7) ensure low-cost scalable fabrication. As a key element for stability and scalable fabrication, we developed porous TiN⁶ for the recording site material. Sites made of this material are compatible with CMOS processing and feature low, uniform impedance ($149 \pm 6\text{ k}\Omega$,

mean \pm s.d., Fig. 1e). Our criterion for long-term stability was good performance up to 8 weeks after implantation, a time frame chosen to ensure that most research questions in rodents, our focus for these probes, can be addressed. We found no stability difference between TiN and standard (PEDOT¹⁷-coated gold) site probes implanted in the rat medial prefrontal cortex (mPFC, Extended Data Fig. 4a–d). Furthermore, probes with and without on-site amplifiers, and with and without switchable sites, all exhibited stable firing rates in the rat mPFC (Extended Data Figs 4e–g and 5). The use of high-throughput silicon fabrication processes to achieve our first six objectives also ensured that Neuropixels probes can be manufactured at low cost and large scale.

Neuropixels probes allowed us to obtain electrophysiological measurements across a large spatial extent with an unprecedented level of detail. In one example, a probe was inserted into the brain of an awake, head-fixed mouse, targeting the primary visual cortex and the lateral posterior nucleus of the thalamus, which receives direct projections from the primary visual cortex¹⁸. Because the probes record activity with the same spatial resolution along the entire shank, the data can be conveniently displayed as images with each site represented as a 'pixel'. Using these images, structural boundaries can be visualized using simple measures of neural activity, such as multi-unit firing rates or signal amplitude in certain frequency ranges (Fig. 2a–c; also see Extended Data Fig. 6). From this recording (Fig. 2d), 206 putative individual neurons were isolated from the cortex, hippocampus, and thalamus using automated spike sorting methods¹⁹ with manual curation²⁰. Regions near the top and bottom of the probe were strongly modulated by visual stimuli (Fig. 2e). Histology revealed that these regions corresponded to the primary visual cortex and the lateral posterior nucleus of the thalamus (Fig. 2f, g).

In a separate example experiment, two probes were inserted into the brain of an awake, head-fixed mouse. One probe spanned the sensory

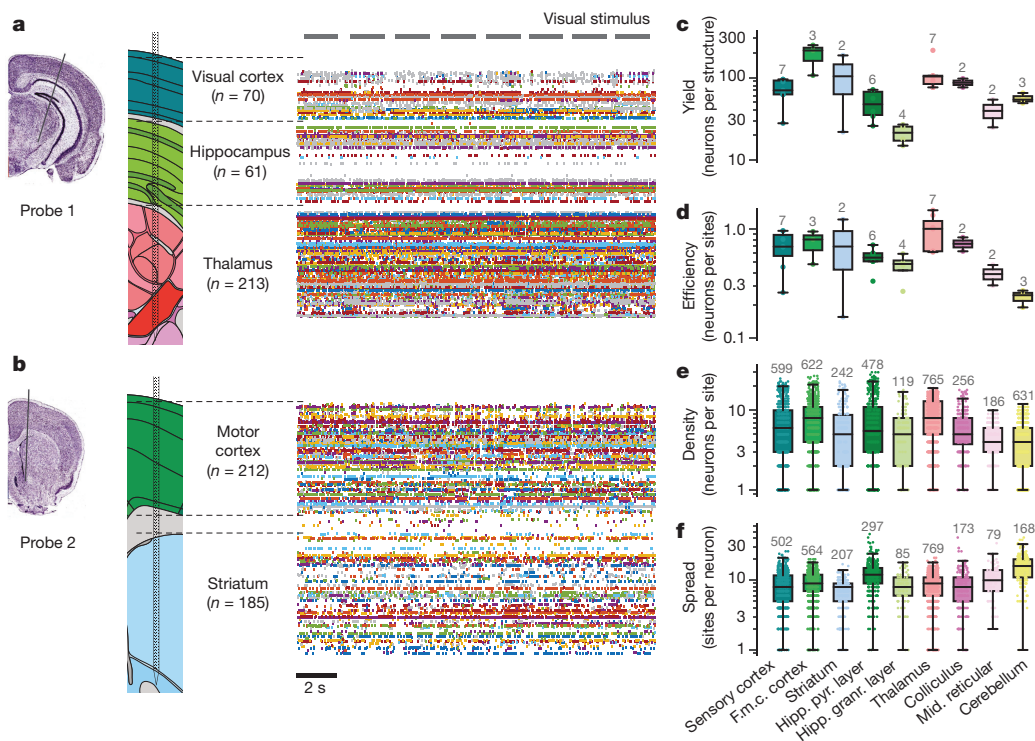


Figure 3 | Recording from multiple brain structures in awake head-fixed mice. **a, b**, Example experiment with two probes recording from five major brain structures. Approximate probe locations are shown overlaid on the Allen Mouse Brain Atlas at the left. A total of 741 putative individual neurons were recorded simultaneously; the number of putative single neurons from each structure is shown in parentheses. **c–f**, Quantification of neuron yield across 9 brain structures ($n = 15$ recordings from 13 mice). For each recording, structure borders were annotated manually based on histological reconstruction or physiological signatures. For each structure, we computed: the total number of putative single neurons (**c**); the efficiency of isolating single neurons (total number

of neurons isolated from a structure divided by the number of sites in that structure) (**d**); the density of neurons per site (number of neurons with median waveform maximum absolute value $>20\mu\text{V}$ for each site) (**e**); and the spread of individual neuron waveforms across the probe (number of channels with median waveform maximum absolute value $>20\mu\text{V}$) (**f**). Box plots show median and quartile range (whiskers denote $1.5\times$ the interquartile range). Individual data points are overlaid (number of points above each plot). F.m.c., frontal/motor/cingulate cortex; hipp. pyr layer, hippocampal pyramidal layer; hipp. granr. layer, hippocampal granule cell layer.

cortex, hippocampus and thalamus (Fig. 3a), whereas the second probe spanned motor cortex and striatum (Fig. 3b). In this experiment, we recorded 741 putative single neurons simultaneously.

Recordings with such high yields were the norm with Neuropixels probes, from both superficial and deep structures. To quantify single neuron isolation across experiments, we compared statistics from recordings made from several laboratories in diverse brain structures such as the cortex, hippocampus, striatum, thalamus, superior colliculus and cerebellum ($n = 13$ mice, 15 experiments). Neuropixels probes allowed isolation of $20\text{--}200$ neurons per structure (79.0 ± 55.5 per structure; Fig. 3c). The number of isolated neurons depended on the number of sites in that region (0.64 ± 0.32 neurons per site; Fig. 3d) and the spatial spread of the waveform of each neuron on the probe. Although most sites sampled signals from multiple (6.9 ± 5.1) neurons (Fig. 3e), good single-neuron isolation was possible because each neuron was visible across 9.5 ± 5.3 sites (Fig. 3f, Extended Data Fig. 7a, b). A neuron appearing on 4–6 sites enables effective sorting¹². Neuropixels probes maintained high signal quality across more than 10 acute insertions (Extended Data Fig. 7c, d).

Because light induces voltage transients in nearly all materials used for extracellular electrophysiology, we tested the sensitivity of Neuropixels probes to optical excitation conditions used for optogenetic perturbations in tandem with extracellular electrophysiology²¹. Direct illumination of the probes in saline resulted in a small, non-saturating artefact that can be minimized using sinusoidal or ramped light pulses (Extended Data Fig. 3c–e) or subtracted out. We were thus able to combine Neuropixels recordings with optogenetic stimulation of both excitatory and inhibitory neuron populations *in vivo* (Extended Data Fig. 8).

A variety of experiments benefit from chronic implantation of silicon probes and recording in freely moving rodents^{22,23}. Owing to their light weight, small footprint and integrated electronics, Neuropixels probes are ideal for such recordings. Although there is a previous report of silicon probe recordings with more than 300 isolated neurons¹⁶, this yield was achieved with a 16-shank array coupled to external amplification and multiplexing electronics requiring large-form-factor hardware, making it impractical to use the probes in freely moving rodents. We monitored activity for at least 8 weeks in a variety of chronic implant geometries. Not only is this sufficient time for most rodent studies, but also the onset of activity loss is usually observed within this time frame²⁴.

We tested chronic implants of Neuropixels probes and obtained large scale single-neuron recordings in both freely moving rats (Fig. 4 and Extended Data Fig. 5) and head-fixed mice (Extended Data Fig. 9). For example, a probe implanted in the rat entorhinal cortex isolated the activity of 127 neurons, including 22 grid cells²⁵, 49 days after implantation (Fig. 4a–c). Similarly, a probe implanted in the rat mPFC delivered low-noise recordings of hundreds of neurons (isolated using another recently developed spike sorting package²⁶) simultaneously for more than 8 weeks (Fig. 4d–g and Extended Data Fig. 5), and a probe implanted in the mouse frontal cortex and lateral septal nucleus delivered stable chronic recordings of more than 100 neurons over more than 150 days (Extended Data Fig. 9b). Across 14 chronic implants in the rat mPFC, we did not observe degradation of spiking activity over 8 weeks (linear regression *t*-test, single-tailed, $P > 0.1$). We have yet to find specific limits to the duration of chronic recordings with Neuropixels and saw no

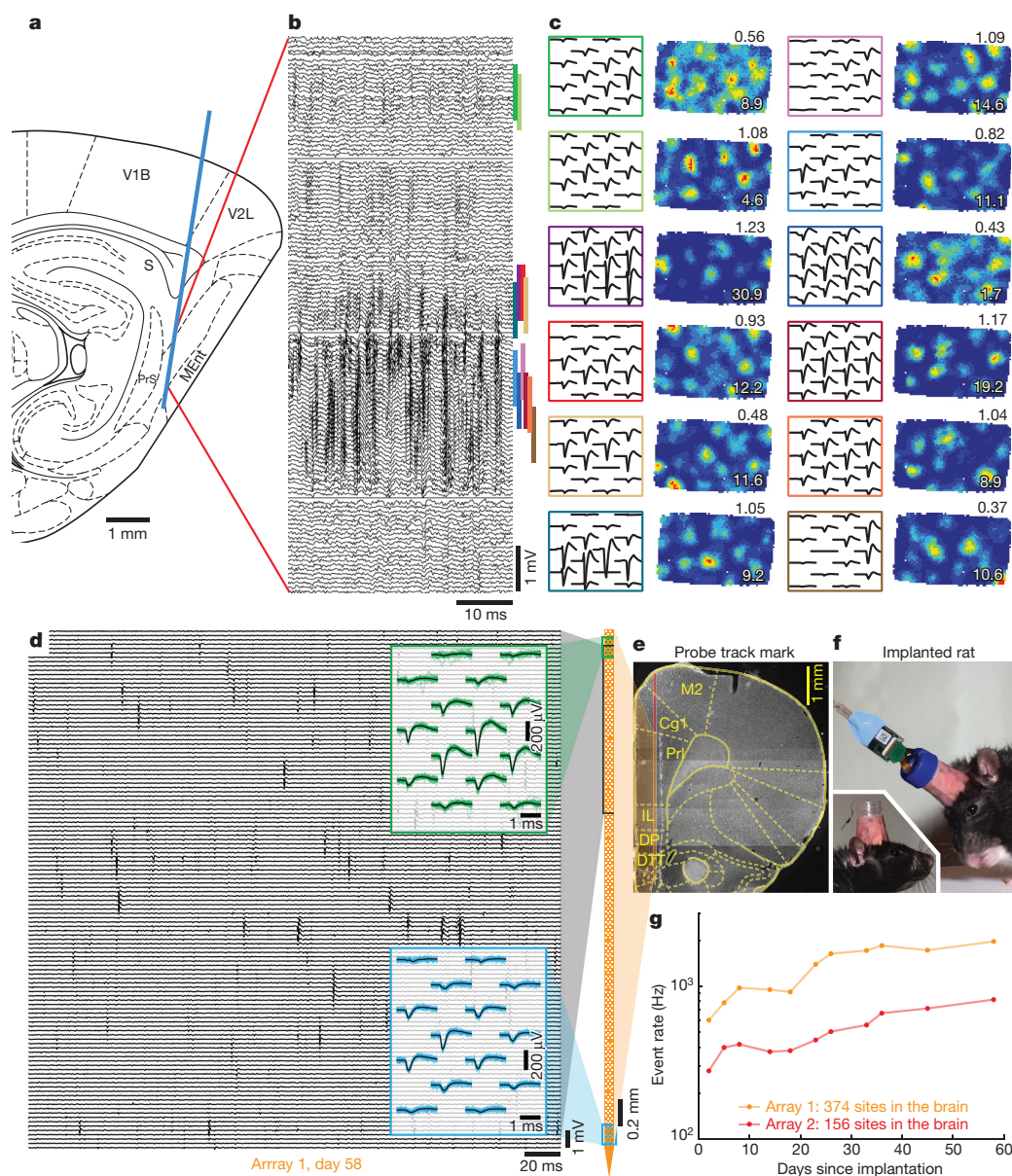


Figure 4 | Recordings from entorhinal and medial prefrontal cortices using chronic implants in unrestrained rats. **a**, Schematic representation of the implant in the entorhinal cortex. MEnt, medial entorhinal cortex; PrS, presubiculum; S, subiculum; V1B, primary visual cortex, binocular area; V2L, secondary visual cortex, lateral area. **b**, Filtered voltage traces from 130 channels spanning 1.3 mm of the shank. **c**, Rate maps and spike waveforms for 12 selected grid cells with a similar grid scale. Colour code corresponds to anatomical location in **b**. Peak firing rate given at bottom of rate maps, grid score³⁰ at top. In total, 127 entorhinal cells were recorded from one rat on day 49 after implantation while it freely foraged for food in a 1.8×1.0 m box. 36 neurons exhibited spatially modulated firing patterns, 22 of which passed the standard grid cell criterion (grid

score above 0.27). **d**, mPFC recording ($n = 3$ rats), 200 ms of voltage traces and examples of waveforms from two sorted neurons. Insets, dark lines show average waveform overlaid with 30 randomly selected single event waveforms of a neuron located at the top (green) and bottom (blue) of the distal most group of 384 sites (array 1). **e**, Anatomical targeting of the chronic implant in mPFC. Section was immunofluorescently labelled with IBA-1. Cg1, cingulate cortex, area 1; DP, dorsal peduncular cortex; DTT, dorsal tenia tecta; IL, infralimbic cortex; M2, secondary motor cortex; Prl, prelimbic cortex. **f**, Photos showing a rat with a chronically implanted Neuropixels probe in the mPFC. **g**, Plot of total event rate (summed over 374 sites for array 1 and 156 sites for array 2) across recording sessions over 60 days. See Methods for further details.

sign that the probes themselves deteriorate (Fig. 4g and Extended Data Figs 5 and 9).

In summary, Neuropixels probes provide an order of magnitude increase in the number of simultaneously recorded neurons obtainable per shank while maintaining low noise. This expanded recording capability has many applications, such as simultaneously monitoring the inputs and outputs of diverse regions (for example, by recording populations in thalamus simultaneously with a target cortical area), as well as assessing the relationship of behaviour to activity distributed across the brain. Moreover, owing to the integrated circuitry for

amplification, multiplexing and digitization, Neuropixels probes have a small physical footprint and minimal cabling, important for studying unrestrained behaviours, and require only a simple interface board to acquire data. More generally, such integration realizes the promise of fully combining advanced, scalable chip fabrication methods with electrode technology. The 1-cm recording length—comparable to the size of the rodent brain—enables recording from multiple brain regions simultaneously at neuronal scale and with high temporal resolution, an essential step towards understanding the global coordination of activity fundamental to brain function^{27–29}.

Online Content Methods, along with any additional Extended Data display items and Source Data, are available in the online version of the paper; references unique to these sections appear only in the online paper.

Received 27 February; accepted 16 October 2017.

- Lewis, C. M., Bosman, C. A. & Fries, P. Recording of brain activity across spatial scales. *Curr. Opin. Neurobiol.* **32**, 68–77 (2015).
- Bargmann, C. *et al.* BRAIN 2025: a Scientific Vision; Brain Research through Advancing Innovative Neurotechnologies (BRAIN) Working Group Report to the Advisory Committee to the Director, NIH. Available at: <http://www.nih.gov/science/brain/2025/> (2014).
- Sofroniew, N. J., Flickinger, D., King, J. & Svoboda, K. A large field of view two-photon mesoscope with subcellular resolution for *in vivo* imaging. *eLife* **5**, e14472 (2016).
- Hamel, E. J. O., Grewe, B. F., Parker, J. G. & Schnitzer, M. J. Cellular level brain imaging in behaving mammals: an engineering approach. *Neuron* **86**, 140–159 (2015).
- Ahrens, M. B., Orger, M. B., Robson, D. N., Li, J. M. & Keller, P. J. Whole-brain functional imaging at cellular resolution using light-sheet microscopy. *Nat. Methods* **10**, 413–420 (2013).
- Musa, S. Titanium nitride electrode. US patent 9,384,990 (2016).
- Buzsáki, G. Large-scale recording of neuronal ensembles. *Nat. Neurosci.* **7**, 446–451 (2004).
- Stevenson, I. H. & Kording, K. P. How advances in neural recording affect data analysis. *Nat. Neurosci.* **14**, 139–142 (2011).
- Meister, M., Wong, R. O. L., Baylor, D. A. & Shatz, C. J. Synchronous bursts of action potentials in ganglion cells of the developing mammalian retina. *Science* **252**, 939–943 (1991).
- Wilson, M. A. & McNaughton, B. L. Dynamics of the hippocampal ensemble code for space. *Science* **261**, 1055–1058 (1993).
- Seymour, J. P., Wu, F., Wise, K. D. & Yoon, E. State-of-the-art MEMS and microsystem tools for brain research. *Microsyst. Nanoeng.* **3**, 16066 (2017).
- Harris, K. D., Henze, D. A., Csicsvari, J., Hirase, H. & Buzsáki, G. Accuracy of tetrode spike separation as determined by simultaneous intracellular and extracellular measurements. *J. Neurophysiol.* **84**, 401–414 (2000).
- Mora Lopez, C. *et al.* A neural probe with up to 966 electrodes and up to 384 configurable channels in 0.13 μm SOI CMOS. *IEEE Trans. Biomed. Circuits Syst.* **11**, 510–522 (2017).
- Scholvin, J. *et al.* Close-packed silicon microelectrodes for scalable spatially oversampled neural recording. *IEEE Trans. Biomed. Eng.* **63**, 120–130 (2016).
- Rios, G., Lubenov, E. V., Chi, D., Roukes, M. L. & Siapas, A. G. Nanofabricated neural probes for dense 3-D recordings of brain activity. *Nano Lett.* **16**, 6857–6862 (2016).
- Shobe, J. L., Claar, L. D., Parhami, S., Bakhurin, K. I. & Masmanidis, S. C. Brain activity mapping at multiple scales with silicon microprobes containing 1,024 electrodes. *J. Neurophysiol.* **114**, 2043–2052 (2015).
- Ludwig, K. A. *et al.* Poly(3,4-ethylenedioxythiophene) (PEDOT) polymer coatings facilitate smaller neural recording electrodes. *J. Neural Eng.* **8**, 014001 (2011).
- Roth, M. M. *et al.* Thalamic nuclei convey diverse contextual information to layer 1 of visual cortex. *Nat. Neurosci.* **19**, 299–307 (2016).
- Pachitariu, M., Steinmetz, N. A., Kadir, S. N., Carandini, M. & Harris, K. D. Fast and accurate spike sorting of high-channel count probes with KiloSort. *Adv. Neural Inf. Process. Syst.* 4448–4456 (2016).
- Rossant, C. *et al.* Spike sorting for large, dense electrode arrays. *Nat. Neurosci.* **19**, 634–641 (2016).
- Yizhar, O., Fenno, L. E., Davidson, T. J., Mogri, M. & Deisseroth, K. Optogenetics in neural systems. *Neuron* **71**, 9–34 (2011).
- Wang, Y., Romani, S., Lustig, B., Leonardo, A. & Pastalkova, E. Theta sequences are essential for internally generated hippocampal firing fields. *Nat. Neurosci.* **18**, 282–288 (2015).
- Buzsáki, G., Horváth, Z., Urioste, R., Hetke, J. & Wise, K. High-frequency network oscillation in the hippocampus. *Science* **256**, 1025–1027 (1992).
- Karumbaiah, L. *et al.* Relationship between intracortical electrode design and chronic recording function. *Biomaterials* **34**, 8061–8074 (2013).
- Hafting, T., Fyhn, M., Molden, S., Moser, M.-B. & Moser, E. I. Microstructure of a spatial map in the entorhinal cortex. *Nature* **436**, 801–806 (2005).
- Jun, J. J. *et al.* Real-time spike sorting platform for high-density extracellular probes with ground-truth validation and drift correction. Preprint at <https://www.biorxiv.org/content/early/2017/01/19/101030> (2017).
- Harris, K. D. Neural signatures of cell assembly organization. *Nat. Rev. Neurosci.* **6**, 399–407 (2005).
- Churchland, M. M., Yu, B. M., Sahani, M. & Shenoy, K. V. Techniques for extracting single-trial activity patterns from large-scale neural recordings. *Curr. Opin. Neurobiol.* **17**, 609–618 (2007).
- Alivisatos, A. P. *et al.* The brain activity map project and the challenge of functional connectomics. *Neuron* **74**, 970–974 (2012).
- Boccaro, C. N. *et al.* Grid cells in pre- and parasubiculum. *Nat. Neurosci.* **13**, 987–994 (2010).

Supplementary Information is available in the online version of the paper.

Acknowledgements We thank the support of the charities that fully funded this work: Howard Hughes Medical Institute's Janelia Research Campus, Allen Institute for Brain Science, Gatsby Charitable Foundation (grant GAT3353), and the Wellcome Trust (grant 100154). We thank S. Caddick for early and continued enthusiastic support of the project. We thank G. Buzsáki for advice and D. Rinberg for early discussions and advocacy. C.M., S.L.G. and C.A.A. would like to thank NSG portal personnel for offering core-hour access to the San Diego Supercomputer Center, troubleshooting and support. The Allen Institute for Brain Science wishes to thank the enduring support of our founders, Paul G. Allen and Jody Allen, without whom this work could not have been accomplished. J.C., C.A. and V.B. were funded by NERF. Experiments and software development in the laboratory of M.C. and K.D.H. were supported by the Wellcome Trust (grants 095668 and 095669). M.C. holds the GlaxoSmithKline/Fight for Sight Chair in Visual Neuroscience. N.A.S. was supported by postdoctoral fellowships from the Human Frontier Science Program and the Marie Curie Actions of the EU.

Author Contributions A.K.L., T.D.H. and B.D. conceived and originated the project. T.D.H., C.K., J.O., M.C., K.D.H., M.H., A.K.L. and K.S. secured project funding. T.D.H., A.K.L., B.D., S.M., C.M.L., J.P., J.O., C.K., T.J.B., J.J.J., N.A.S., J.H.S., D.J.D., M.Bau, B.B., D.A.G., K.D.H., M.H., B.K., P.L., P.D.R. and K.S. determined specifications. A.A., C.M.L., S.M., J.P., W.S. and T.D.H. designed and produced devices and firmware. J.J.J., N.A.S., J.H.S., D.J.D., B.B., T.J.B., B.K., P.L., C.M.L., S.M., J.P., W.S. and T.D.H. tested devices *in vitro*. N.A.S., J.H.S., D.J.D., M.Bar, V.B., C.A. and J.C. performed acute recordings in mouse or rat. J.J.J. and P.D.R. performed chronic recordings in the rat mPFC. M.Bau performed chronic recordings in the rat entorhinal cortex. N.A.S. and M.O. performed chronic recordings in mouse. J.J.J., N.A.S., J.H.S., M.Bau, B.B., T.J.B., C.M.L., S.M., J.P. and W.S. developed instrumentation or other materials. J.J.J., N.A.S., J.H.S., D.J.D., M.Bau, B.B., A.K.L., M.Bar, T.J.B., V.B., M.C., J.C., D.A.G., K.D.H., M.H., P.L., J.O., M.O., P.D.R., K.S. and T.D.H. designed experiments. B.K., J.P., J.H.S., D.J.D., J.J.J., M.P., K.D.H. and C.R. wrote software for data acquisition or analysis. C.A.A., S.L.G. and C.M. performed simulations. J.J.J., N.A.S., J.H.S., D.J.D., M.Bau, B.B., C.A. and J.C. analysed data. T.D.H., A.K.L., M.C., N.A.S., D.J.D., C.K., J.J.J., J.H.S., M.Bau, V.B., J.C., K.D.H., C.M.L., B.D. and J.O. wrote and edited the manuscript with input from all authors. J.J.J., N.A.S., J.H.S., D.J.D., M.Bau, B.B. and J.C. prepared figures. T.D.H., B.D., M.C., J.O., T.J.B., K.D.H., D.J.D., V.B., C.K. and K.S. supervised the work. T.D.H. and S.M. managed the project.

Author Information Reprints and permissions information is available at www.nature.com/reprints. The authors declare no competing financial interests. Readers are welcome to comment on the online version of the paper. Publisher's note: Springer Nature remains neutral with regard to jurisdictional claims in published maps and institutional affiliations. Correspondence and requests for materials should be addressed to T.D.H. (harrist@janelia.hhmi.org).

Reviewer Information *Nature* thanks M. Maharbiz and the other anonymous reviewer(s) for their contribution to the peer review of this work.

METHODS

No statistical methods were used to predetermine sample size. The experiments were not randomized, and investigators were not blinded to allocation during experiments and outcome assessment.

Impedance measurements. Impedance measurements were performed *in vitro* for all phase 1 probes, for phase 2 passive switched and unswitched probes, and for passive unswitched phase 3 probes (Fig. 1e) (see Supplementary Information for details on the development phases). For phases 1 and 2, the probe was immersed in PBS and connected to a nanoZ impedance analyser (White Matter LLC) 32 channels at a time. Measurements were done at 1 kHz only and the system was calibrated with resistive loads. For phase 3, an impedance-measurement circuit was included in each recording channel to estimate the electrode impedance at a selected frequency of 1 kHz. The circuit consisted of a square current signal generator placed at the input terminal of the recording channel, which directly delivered a current with an amplitude of 1 nA to the selected electrodes. The voltage generated at the channel input was then monitored by the readout circuits as in normal operation. With this circuit we could measure electrode impedances in a range of 100 k Ω to 10 M Ω , with an accuracy of $\pm 20\%$. These measurements were done inside a Faraday cage, using the external reference connected to ground, and selecting a channel amplifier gain of 250.

Acute experiments. Acute recordings were performed at the Allen Institute for Brain Science (AIBS) and at University College London (UCL) with slightly different procedures, described below. Surgeries and experimental procedures at AIBS were approved by the AIBS Institutional Animal Care and Use Committee. Experimental procedures at UCL were conducted according to the UK Animals Scientific Procedures Act (1986) and under personal and project licenses released by the Home Office following appropriate ethics review.

For awake, head-fixed recordings (Figs 2, 3c–f and Extended Data Figs 1, 7 and 8), mice were male C57BL/6 or Rorb-Cre;Ai32 (expressing ChR2 primarily in L4 of cortex). An initial surgery was performed to attach a headpost to the skull. After recovery, each animal was habituated to the experimental apparatus. The apparatus consisted of a horizontal disc suspended in a spherical environment onto which images were projected; animals were head-fixed on the disc and allowed to run at will. On the day of recording, the animal was anaesthetized with isoflurane and one or more craniotomies were made. A skull screw was implanted rostrally for use as the recording reference. The animal was transferred to the experimental apparatus and allowed to recover from anaesthesia. One or two probes were lowered through the craniotomies manually, piercing the dura mater. After smooth descent to the final depth, probes were left untouched for a minimum of 30 min before any recording. When applicable, visual stimulation was provided to drive activity in the underlying structure. For some recordings (Extended Data Fig. 1a, b), probes were connected to commercial electrophysiology recording hardware (eCube, White Matter LLC). The eCube system amplified ($200\times$ gain) and digitized (25 kHz, 14 bits) at 0.61 μ V per bit resolution.

For awake, head-fixed mouse recordings (Fig. 3 and Extended Data Figs 7 and 8), mice were C57BL/6J or transgenic; in particular, for optogenetic experiments (Extended Data Fig. 8) and some other recordings (Fig. 3, Extended Data Fig. 7), PV-Cre;Ai32 mice (expressing ChR2 in Pvalb-positive inhibitory interneurons) were used. Mice were male or female, between 2 and 8 months of age. In all cases, a brief (<1 h) surgery to implant a steel headplate was first performed. Following recovery, mice were acclimated to head-fixation in the recording setup. During head-fixation mice were seated on a plastic apparatus with forepaws on a rotating rubber wheel. Three computer screens were positioned around the mouse at right angles. On the day of recording, mice were again briefly anaesthetized with isoflurane while one or more craniotomies were made, either with a dental drill or a biopsy punch. After several hours of recovery, mice were head-fixed in the setup. Probes had an Ag wire soldered onto the reference pad and shorted to ground; these reference wires were connected to an Ag/AgCl wire positioned on the skull. The craniotomies as well as the wire were covered with saline-based agar. The agar was covered with silicone oil to prevent drying. In some experiments a saline bath was used rather than agar. Electrodes were then advanced through the agar and through the dura. Electrodes were allowed to settle for approximately 20 min before starting recording. For optogenetics experiments, 473 nm light was generated by a diode laser (LuxX, Photon Lines Ltd) and passed through an optical fibre before a lens focused the light to a spot $\sim 150\mu$ m in diameter on the surface of the brain near the probe. Light was delivered in a 40 Hz raised cosine wave pattern, with peak light power at the surface of the brain of approximately 1.5 mW. Acute recordings at both AIBS and UCL were made in external reference mode with LFP gain = 250 and AP gain = 500.

These data were automatically spike sorted with the Kilosort spike sorting software¹⁹ and then manually curated with the 'phy' gui (<https://github.com/kwikteam/phy>). During manual curation, each set of spikes detected by a particular template was compared to those from similar templates to determine whether, on

the basis of spike waveform similarity, drift patterns, or cross-correlogram features, they should be merged. Then, the spikes of each template were assessed qualitatively in terms of the spike amplitude, waveform consistency, presence of short-latency ISIs, and presence of any similar nearby neurons. If satisfactory on all counts, the spikes were included in the quantification of Fig. 3 and Extended Data Fig. 7.

Recordings from head-fixed locomoting mice were performed at NERF, Leuven Belgium. Experiments were performed in compliance with protocols approved by the ethical research committee of the Katholieke Universiteit of Leuven. Eight C57BL/6J mice (~ 22 – 30 g, ~ 2 – 4 months old at the time of surgery) of either gender were prepared for acute recording sessions (4 with passive option and 4 with active option probes) following similar procedures described previously³¹. In brief, mice were injected with dexamethasone (3.2 mg kg⁻¹ intramuscularly, 4 h before surgery) and anaesthetized with isoflurane (induced 3%, 0.81 min⁻¹ O₂; sustained 1–1.5%, 0.51 min⁻¹ O₂). A custom-made head-plate was attached to the skull using adhesive cement and the skull over visual cortex was covered with glue (VetBond, 3M) and silicone sealant (KwikCast, World Precision Instruments).

Mice were habituated to the recording setup for at least 2 weeks and were again anaesthetized with isoflurane, a stainless steel ground screw was implanted over the cerebellum and a craniotomy was made above visual cortex using stereotaxic coordinates (3.8 mm caudal, 2.5 mm lateral from bregma). The craniotomy was covered with artificial dura (3-4680, Dow Corning) and silicone sealant (KwikCast, World Precision Instruments). Mice were allowed to recover for at least one day before recording. The behavioural setup consisted of a treadmill built with an optical encoder (Avago Technologies) attached to the shaft of the wheel to monitor belt movement at a precision of 1.20 mm. A photoelectric sensor (Omron) controlled the release of a water reward ($\sim 2.5\mu$ l) every 150 cm. The encoder and photoelectric signal were recorded simultaneously by Presentation (Neurobehavioural Systems) and the Whisper system (<https://www.janelia.org/lab/harris-lab-apig/apig-research/extracellular-electrophysiology>) was used to record neuronal signals. For recording, mice were head-fixed and the silicone sealant removed. A passive or active option phase 2 probe was attached to a micromanipulator (Scientifica) and placed perpendicular to the brain surface. The probe was lowered (1.25–1.35 mm below pia) at 1–2 μ m s⁻¹. The craniotomy was then covered with 1% agarose and recordings initiated after a waiting period of at least 30 min. After recording, the probe was slowly retracted and the craniotomy resealed. Recordings lasted three sessions or until unit yield in superficial layers decayed substantially. Spike sorting for Extended Data Fig. 1c–f was performed with JRCLUST²⁶. Further analysis was performed in Matlab (Mathworks) and/or Python using custom written software.

Chronic experiments. Entorhinal cortex implants in rats. These experimental procedures were conducted at UCL according to the UK Animals Scientific Procedures Act (1986) and under personal and project licenses granted by the Home Office following appropriate ethics review. One male Lister Hooded rat was used for chronic recordings, weighing 400 g at time of surgery and maintained on a standard food deprivation schedule and a 12:12 h light:dark schedule. A custom 3D printed holder was designed to house the probe and provide a fixation point for the stereotaxic surgery frame. No microdrive was used. To protect the electric components the probe body was encapsulated in epoxy (Araldite Rapid). During the implantation procedure, the probe was secured in the stereotaxic frame, yaw and pitch axes were adjusted to assure that the probe shank was perpendicular to the horizontal plane through bregma and lambda. A hole for the ground screw was drilled in the right frontal plate and five additional screws were distributed around the implant site (4.3 mm lateral to the midline; 0.3 mm anterior to the sinus) to provide anchoring for dental acrylic. The whole surface of the skull except the implant location was covered with Super-Bond cement (Sun Medical). A 2.4 mm craniotomy was drilled over the implant location and bone was carefully removed. A flap of dura was lifted and a small incision was made to facilitate the probe insertion. The probe was slowly lowered (10–20 μ m s⁻¹) until it reached the target location. The probe shank above the brain surface was covered with Vaseline. The probe was then fixed to the skull using dental acrylic. A copper mesh cage was attached to the probe holder and connected to the skull screw to shield the probe assembly from external noise. The probe's ground and reference were connected to the skull screw. Infrared light-emitting diodes (LEDs) were fixed on the implant in order to track the animal's position.

Spatial response fields were measured in a rectangular-shaped (180 \times 100 cm) smooth-walled wooden box with a white cue card outside the north wall. The rat was transported from the holding platform in the same room into the box using standardized procedures to provide directional constancy. While in the box, the rat searched for randomly distributed grains of sweetened rice.

Recordings were made in external reference mode with LFP gain = 500 and AP gain = 1,000 or 1,500. Recordings were automatically sorted offline using Kilosort software¹⁹. Firing-rate maps were estimated by dividing the number of spikes by the rat's dwell time in a given location bin (3 cm square). Adaptive smoothing was applied to the dwell time and spike maps before dividing them.

mPFC implants in rats. These procedures were conducted at the Janelia Research Campus and approved by the Janelia Institutional Animal Care and Use Committee (IACUC Protocol number: 15-122).

The probe shank was aligned to the axis of penetration on a three-axis micro-manipulator (M3301R Manual Manipulator, World Precision Instruments). The aligned probe was affixed with cyanoacrylate glue (Loctite SuperGlue Gel control) to a mounting block, which was held by a screw to a stereotaxic rod (Kopf Model 1900).

We used male Wistar and Long Evans rats 12–16 weeks old at the time of the implant surgery. Animals were individually housed on a 12-h light/dark schedule with ad libitum access to water. Animals were placed under a reduced calorie intake protocol by limiting the food intake to 15–20 g per day. Body weights were maintained above 85–90% of the animals' initial weights.

Animals were anaesthetized with isoflurane. After clearing the skull a thin layer of light-cured glue (Optibond All-in-one, Kerr) was applied. The ground screw was implanted above the right cerebellum. A thin layer of light-cured adhesive (Charisma A1, Heraeus Kulzer) was applied around the site of implantation (mPFC: 3.24 mm AP, 0.6 mm ML; 4–6 mm DV) and its surface was textured. A 2-mm diameter craniotomy was drilled and the dura was carefully removed using a tissue pick (Fine Science Tools 18067-11) without breaking the arachnoid mater. The probe was inserted by moving it up and down repeatedly while in contact with the arachnoid until the membrane eventually punctured. The probe was slowly lowered ($5\text{--}10\ \mu\text{m s}^{-1}$) to minimize tissue damage. We passed the target depths ($z = 6\text{ mm}$ for a 10 mm shank and $z = 4\text{ mm}$ for a 5 mm shank) by $100\ \mu\text{m}$ then retracted the probe to reduce tissue compression. The craniotomy was kept hydrated with sterile physiological saline solution during the probe descent. Once the probe reached the desired target, the saline was drained and the craniotomy covered with artificial dura (Dow Corning Silicone gel 3-4680). The exposed part of the probe shank was protected by surrounding it with a layer of petroleum jelly (Vaseline). A low-temperature cauterizer was used to pick up and deposit Vaseline by melting it around the shank without directly contacting it. Dental acrylic was then applied to cement the probe to the skull, and the mounting rod was released after the cement had fully cured (10 min). The ground wire of the probe was attached to the ground screw, and both were attached to a copper mesh cone using conductive copper tape. The cone was then cemented onto the skull using dental acrylic and a plastic tube with screw cap was attached to the top.

Recordings began after the two-day recovery period and were repeated 1–2 times per week for 60 days after the implantation. Each recording session lasted for 5–10 min per configuration setting. The screw cap was removed and a recording headstage was securely locked to the tubing threads before attaching the probe flex cable to a ZIF connector on the headstage. Animals were placed on a soft cushion supported by a raised platform and surrounded by walls on four sides ($60 \times 60 \times 150\text{ cm}$). This chamber was brightly lit by white LED light (30 W). The weight of the recording headstage and cables were supported by a counterweight connected to a pulley. After placing the animals within the chamber and plugging the probe into the recording system, recordings were begun 10–15 min after animals exhibited minimal movements.

Recordings were made with custom-written software (<http://billkarsh.github.io/SpikeGLX/>). Phase 1 and 2 probes, which lack on-chip digitizers, were connected to custom-built hardware (<https://www.janelia.org/lab/harris-lab-apig/apig-research/extracellular-electrophysiology>) called WHISPER, based on Intan analogue amplifiers (Intan RHD2132) and NI digitizers (National Instruments NI-DAQmx). The WHISPER system amplified ($200\times$ gain) and digitized (25 kHz, 16 bits) signals at $0.305\ \mu\text{V}$ per bit resolution. Phase 3 recordings used a gain of 500 for the AP band (300 Hz high-pass filter) and a gain of 250 for the LFP band (1 kHz low-pass filter). The external reference setting was used with the skull screw as a signal ground and reference. The chronic recordings from mPFC were processed by the spike sorting pipeline developed at Janelia Research Campus, JRCLUST²⁶. In particular, the raw traces were processed with a Savitzky-Golay filter (quadratic first derivative, 9 taps) and local common average referencing (local CAR). Local

CAR is the subtraction from each site of the mean of four other sites, chosen within a $30\text{--}50\ \mu\text{m}$ radius but excluding immediate neighbours (that is, for each site the 9 nearest sites were identified, then the mean of the sixth to ninth nearest sites was subtracted). Targeting of the recordings was verified by post mortem histology. Slices were immunofluorescently labelled with IBA-1 (Wako 019-19741, lot SAL6018) and imaged (Fig. 4e).

To test the sensitivity of our probes to physical impact, we applied reproducible impacts to the implant cap and measured the resulting accelerations and artefacts. The impact was generated by bending a nylon zip tie (30 cm length, 5 mm width, 1 mm thickness) by 90° and hitting the implant with the blunt end of the zip tie. The consistency of the impacts was checked with an accelerometer mounted onto the implant. For each technology tested, left side sites were recorded with external reference, 187 of 374 recording sites for options 1–3, and 137 out of 274 for option 4, while right side sites were recorded with internal reference, also 187 out of 374 sites for options 1–3, and 137 out of 274 for option 4. These reference choices are selectable parameters for each site, so that the recording is a single trial for both reference choices; internal and external referenced data can therefore be compared directly. The common average reference correction to external referenced data, Extended Data Fig. 2, was far superior, so internal referenced data are not shown.

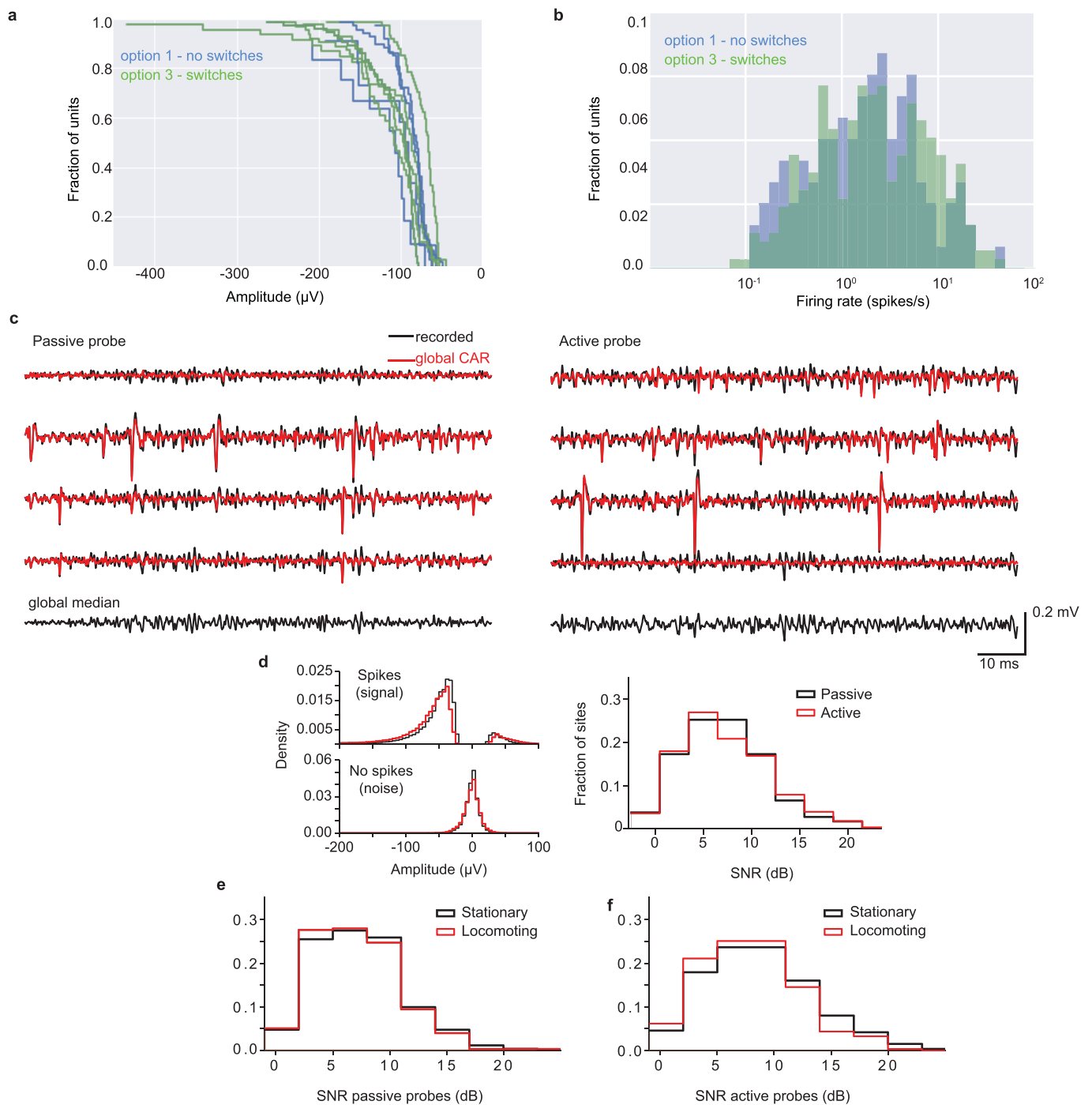
To assess stability across time for chronically implanted probes (Extended Data Figs 4 and 5), we computed the rate of putative neuronal spikes sufficiently above the noise floor ('event rate'). We define an event as temporally coincident (within 1 ms) spikes recorded on a spatially contiguous group of sites ($\sim 50\ \mu\text{m}$ radius) for which the maximum amplitude (negative peak) on any site in the group exceeds the threshold. The threshold was defined as 6 times the MAD (the median absolute deviation). An SNR is calculated for each spike event. The event SNR is the ratio of peak amplitude of the site with largest amplitude (negative peak) in the event to $0.6745 \times \text{MAD}^{32}$. The average event SNR is stable across recording sessions even though there is variation of event rate between sessions (PEDOT-1) (Extended Data Fig. 4c, d). The rate of events in a particular recording session was defined as the total event count divided by the duration of the recording.

Chronic implant in a mouse. This experiment (Extended Data Fig. 9) was performed at UCL and surgical procedures were as described for acute mouse recordings, above, including the implantation of a steel headplate. The basic implantation strategy has been described previously³³. In brief, the mouse was anaesthetized and a small craniotomy was made. The probe, an option 1 probe with Ag reference-wire soldered on and shorted to ground, was held by the PCB and advanced into the opening while recording. When in place, a small amount of Kwik Cast was applied to surround the remaining exposed part of the probe shank. Acrylic was applied to encase the Kwik Cast and connect the probe PCB to the skull and the super-bond comprising the rest of the implant. A custom-designed 3D-printed shell, shaped roughly like a rectangular prism, was lowered over the probe PCB. This shell served to protect the probe and provided a place to tuck the flex ribbon and Ag reference wire into while the mouse was in the home cage. The shell was secured to the implant with more acrylic. The flex was stored in the shell and covered with Micropore tape. The total implant weight was $\sim 3.0\text{ g}$, and the height was $\sim 3\text{ cm}$ (Extended Data Fig. 9a).

For subsequent recordings, the mouse was head-fixed in the same apparatus as described for the acute recordings. The Ag reference wire was connected to the headplate. Recordings were made in external reference mode with LFP gain = 250 and AP gain = 500. Data were processed with Kilosort spike sorting software¹⁹.

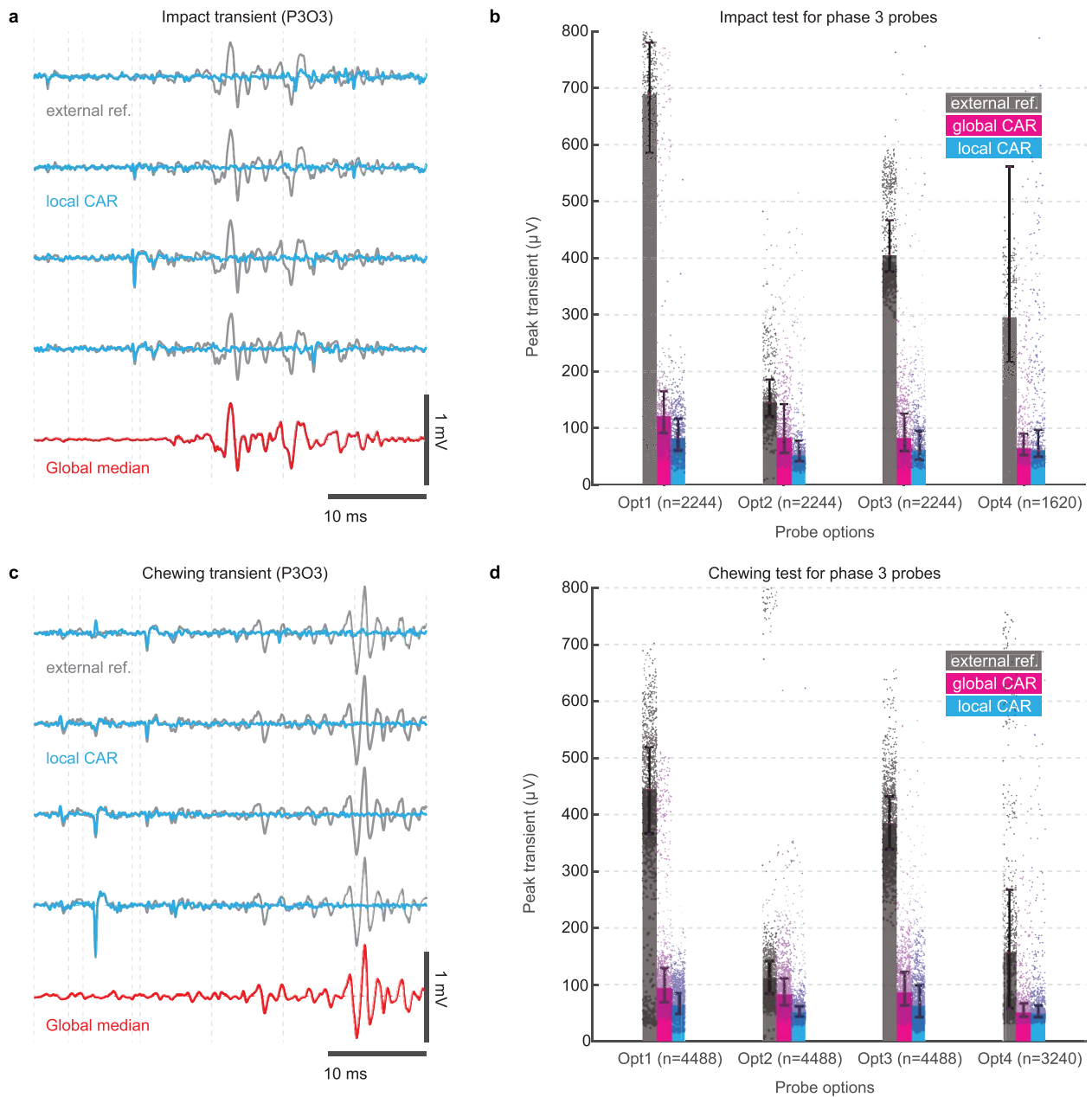
Data availability. All data are available from the corresponding author upon reasonable request.

31. Goldey, G. J. *et al.* Removable cranial windows for long-term imaging in awake mice. *Nat. Protocols* **9**, 2515–2538 (2014).
32. Quiroga, R. Q., Nadasdy, Z. & Ben-Shaul, Y. Unsupervised spike detection and sorting with wavelets and superparamagnetic clustering. *Neural Comput.* **16**, 1661–1687 (2004).
33. Okun, M., Lak, A., Carandini, M. & Harris, K. D. Long term recordings with immobile silicon probes in the mouse cortex. *PLoS One* **11**, e0151180 (2016).



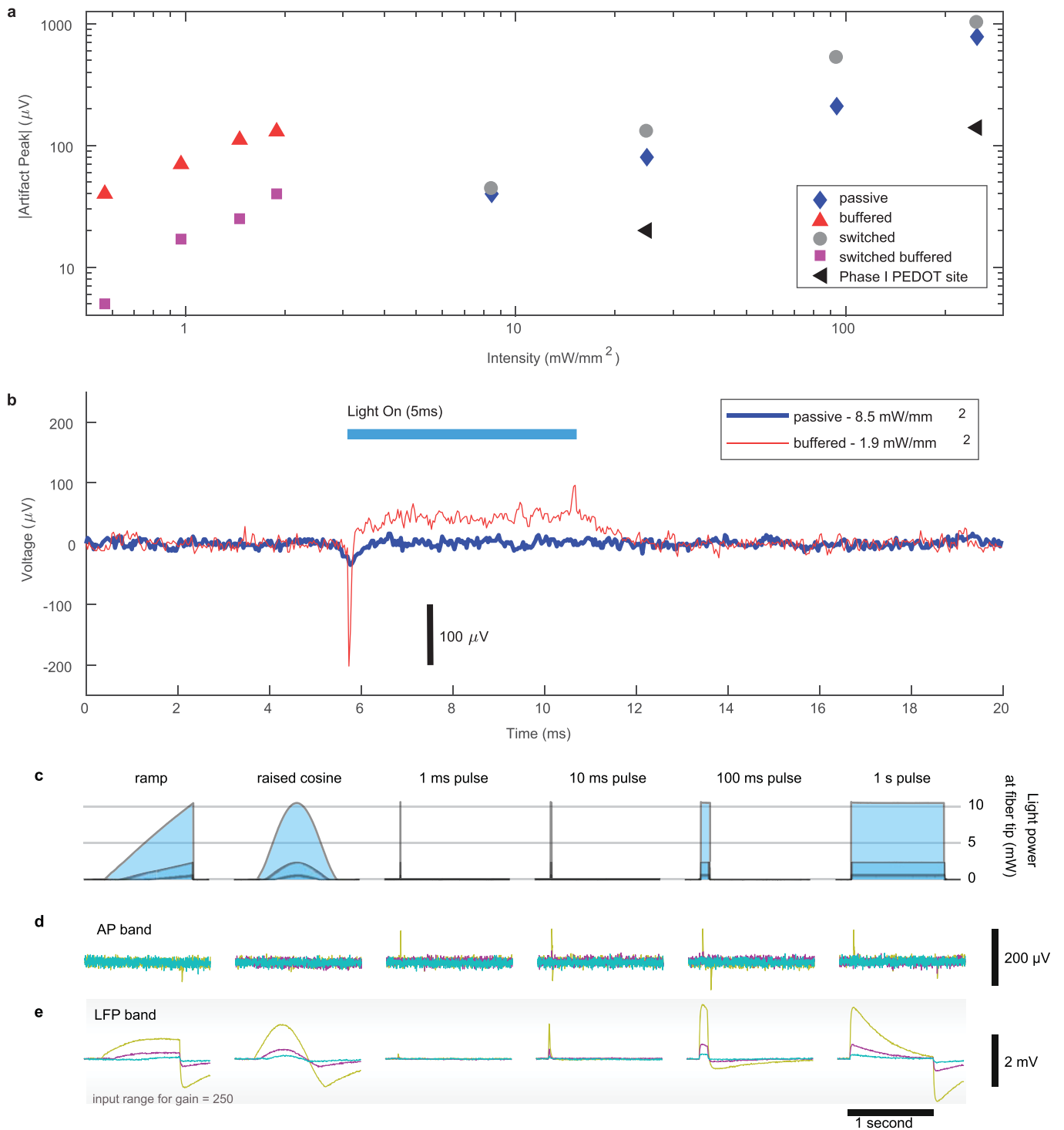
Extended Data Figure 1 | Comparison of switchable and active probe options. **a**, Cumulative distribution of the single unit peak amplitude from recordings using non-switchable (option 1, blue, $n = 5$ recordings) or switchable (option 3, green, $n = 5$ recordings) probes. Each distribution shows an individual recording session; sessions were spike sorted, and the mean waveform on every channel for each unit was computed. The largest absolute peak in the mean waveform on any channel was taken as the amplitude. **b**, Distribution of mean firing rate across the recording sessions for each sorted unit from non-switchable (blue, $n = 119$ cells) and switchable (green, $n = 294$ cells) probes; all recordings with each variant are combined. Switches did not have an appreciable effect on the amplitude or firing rate of recorded units. **c**, Artifacts in awake head-fixed locomoting mice are similar across passive and active probe options and can be removed by common (median) average referencing. Filtered traces (bandpass 300–3,000 Hz) of 4 channels sampled at different depths (grey) and corrected common average referenced (CAR) traces (red). The CAR corrected traces are obtained by subtracting from each trace the median

across all 120 channels (bottom). Figure panel depicts representative examples of artefacts found on both probe options. **d**, Extracellular spike waveform amplitude (signal), noise amplitude, and spike signal-to-noise ratio (SNR) measured in the cortex *in vivo* using passive (black) or actively amplified (red) recording sites. Voltage amplitudes are sampled from 250,000 spikes across the entire probe for each experiment (4 experiments with passive (SNR = 8.78 ± 0.52 , 95% confidence interval) and 4 with active (SNR = 8.95 ± 0.54) recording sites). Signal-to-noise (right) distributions are similar; $P = 0.78$, two-sided Wilcoxon rank-sum. **e**, **f**, Signal-to-noise ratio computed using 200,000 spikes during locomotion (red) or stationary (black) epochs. Recordings with passive sites (3 recordings) are depicted in **e** and recordings with active sites (4 recordings) in **f**. SNR distributions are similar during stationary and locomotion epochs with both probe options. Overall, the performance of probes with on-site buffer amplification is similar to that of probes with passive sites and offers no clear advantage *in vivo*.



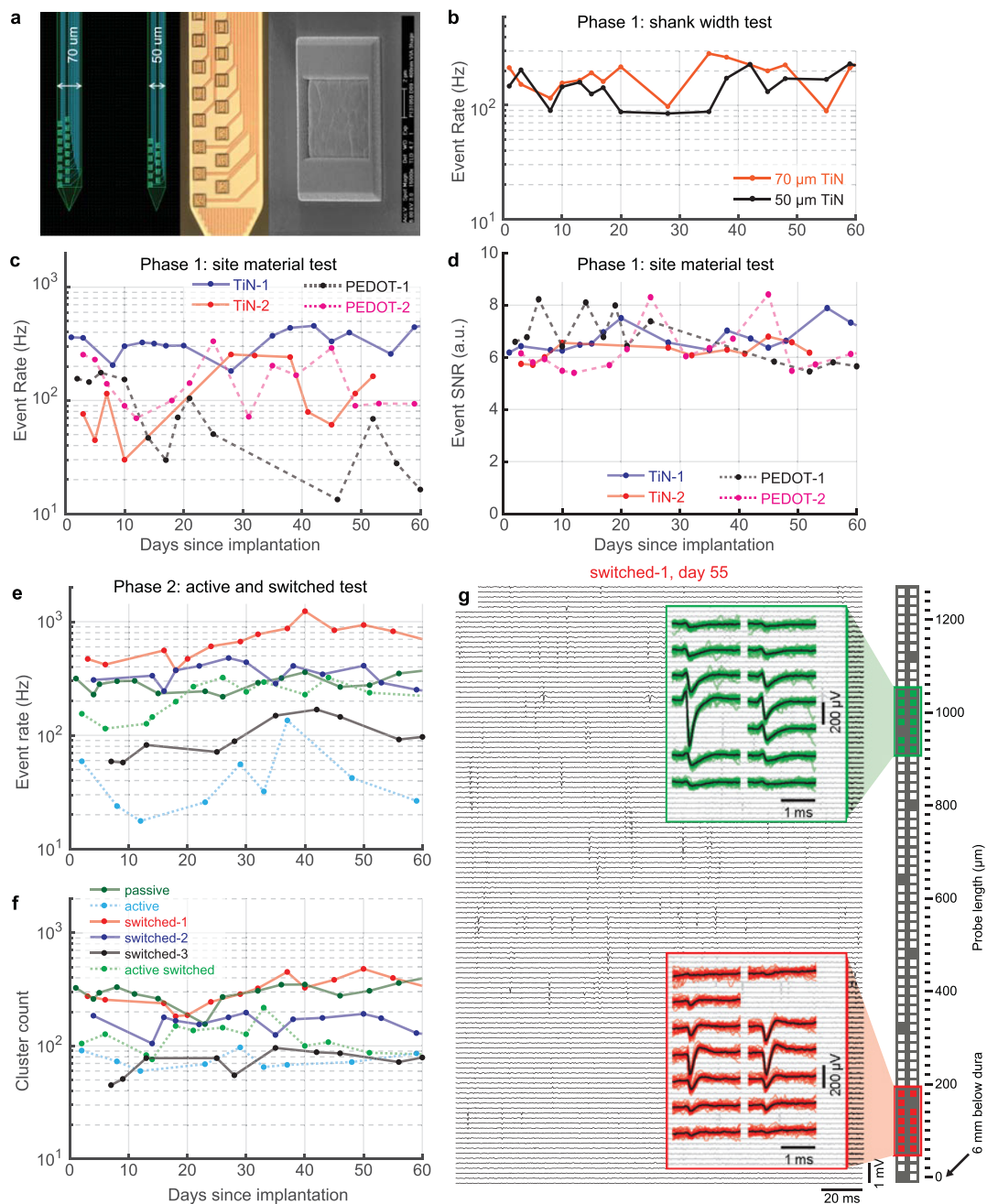
Extended Data Figure 2 | Impact and chewing transient rejection. Reduction of interfering transients with CAR post-processing in software. Recordings using external reference on one animal, 6 or 12 trials for each technology option. **a**, Example signal traces for a phase 3 unbuffered, switched probe in a chronically implanted rat tapped with a cable tie. Shown is the median across all 374 recording sites (red), the raw traces (grey, from 4 adjacent sites), and traces corrected with local CAR (blue; see Methods). **b**, Impact transient magnitudes for all 4 probe options chronically implanted with external referencing, and corrected with global or local CAR ($n=6$ trials, one animal, median \pm interquartile

range). Probes with unity-gain buffer amplifiers at the sites (options 2 and 4) offer no significant advantage for CAR-processed data over probes without buffers (options 1 and 3). **c**, Transients as in **a**, induced by chewing food. **d**, Comparison of all 4 options, as in **b**, one animal. Again, there was no significant advantage to buffer amplifiers after CAR correction (two-sample t -test, $P=0.1266$, $\alpha=0.05$, one-tailed). The median and interquartile ranges are computed from 12 chewing events measured at 270 sites (option 4) or 374 sites (options 1–3). n in **b** and **d** represents the number of independent samples (number of sites \times number of trials). See Methods for details.



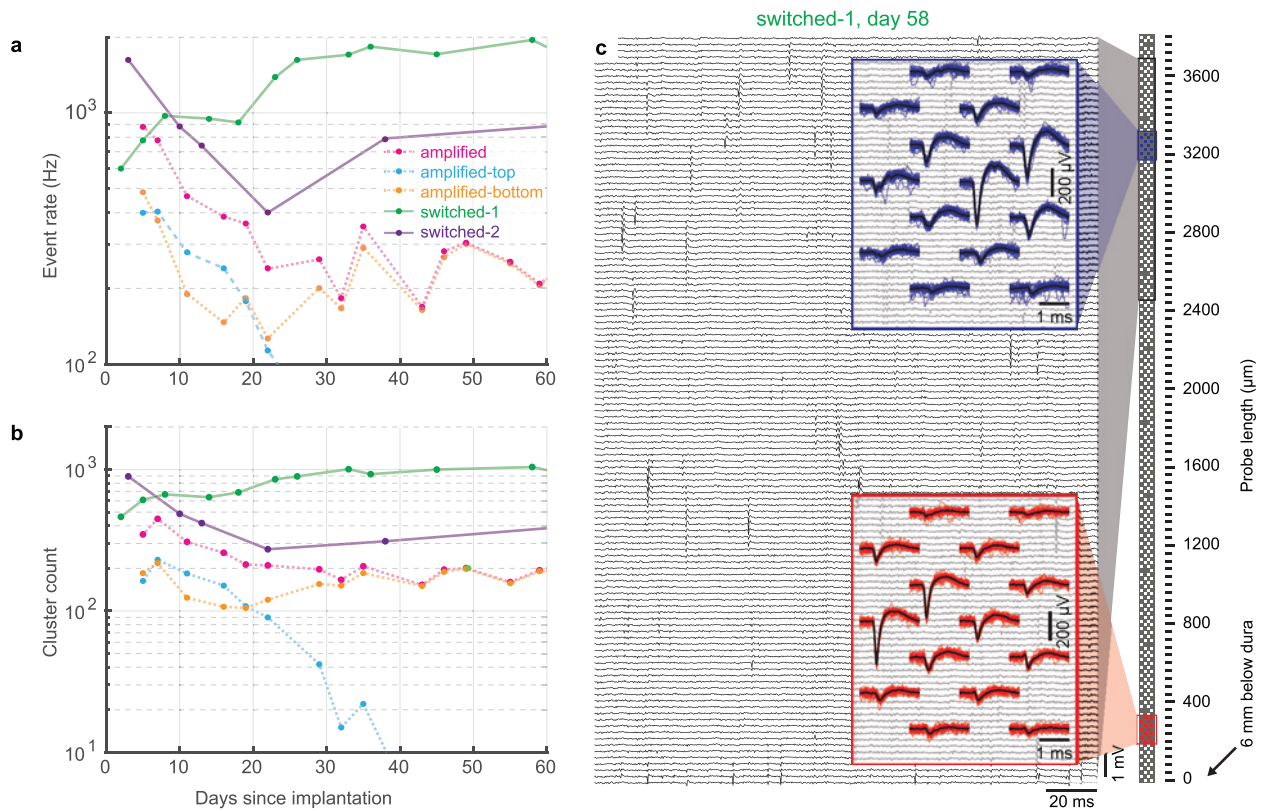
Extended Data Figure 3 | Light sensitivity tests. a, b, A comparison of the light sensitivity of active and passive Neuropixels probes, along with 'conventional' Si probes. **a**, Plot of transient amplitude versus illumination power density for a 5-ms directly applied 473-nm light pulse. Active sites, especially unswitched, were most sensitive. Switched and unswitched passive probes were much less sensitive. In each measurement the 5-ms light pulse was applied singly or in a pulse train at 20 Hz for 1 s. **b**, Example response to illumination with a 5-ms pulse at the indicated power density. In all cases, probes were illuminated with light from a 100- μm core multimode fibre with the probe immersed in phosphate buffered saline. Below intensities of 10–20 mW mm^{-2} directly onto the probe, there is no impact on spike detection (see Extended Data Fig. 8) or

LFP phase or magnitude determination for passive switched Neuropixels probes. Experiments in **a** and **b** were performed once for each probe type. **c–e**, Neuropixels recording sites were immersed in saline and directly illuminated with blue (465 nm) LED light from a 200- μm diameter, 0.66 numerical aperture (NA) fibre optic cable. Light was delivered with 6 different pulse shapes (ramp, raised cosine, square 1 ms, 10 ms, 100 ms and 1 s) at 3 peak power levels. **c**, Light power measured with an amplified photodetector for all 18 pulse types. **d, e**, Artefacts on a representative photodetector for low (cyan traces), middle (magenta traces) and high (yellow traces) light levels. For reference, the input range of the LFP band (gain of 250 \times) is overlaid across the LFP plots.



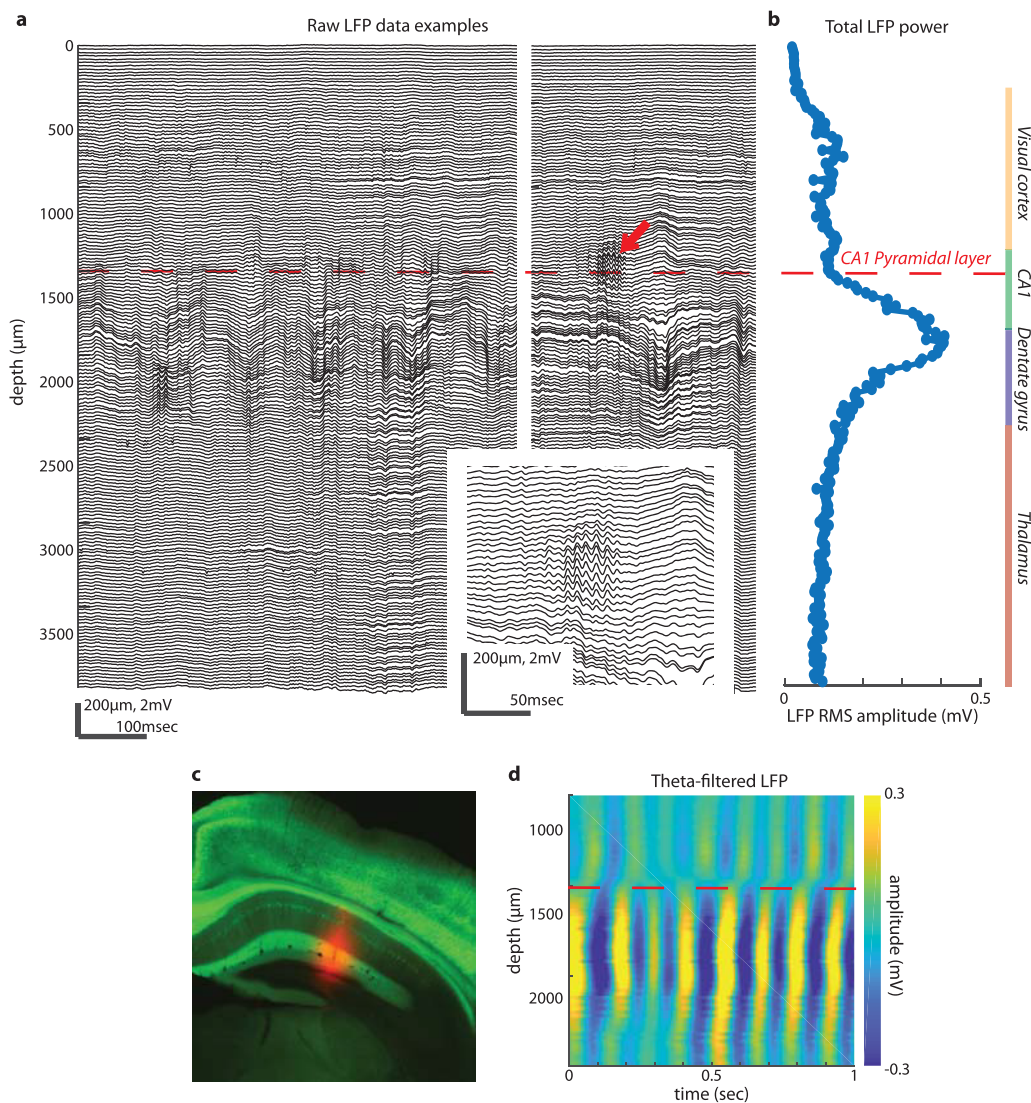
Extended Data Figure 4 | Long-term stability studies: effects of shank width, TiN sites and active and switched sites. **a–d**, To compare the chronic performance of 50- μm wide and 70- μm wide shanks as well as TiN and poly(3,4-ethylenedioxythiophene) (PEDOT)-coated gold sites, four-shank probes with two shanks of each width were constructed. One version had PEDOT-coated gold sites, and a second had TiN sites. These were tested in separate animals. **a**, A diagram of the probe geometry for both probes, two of four shanks, a photograph of the distal end of a TiN site shank, and an electron microscopy image of one TiN site. The site is $12 \times 12 \mu\text{m}$. These probes were chronically implanted in the rat mPFC and recorded in unrestrained animals, without advancing the electrodes, in multiple sessions over a period of 6–8 weeks (further implantation, recording and analysis details are described in the Methods). **b**, The event rate versus implant age for one of two rats with TiN probes in the mPFC. We define an event as time-coincident spikes recorded on a contiguous group of sites for which the maximum amplitude on any site in the group exceeds the threshold. **c**, The event rate versus implant age

for four rats with one probe each in mPFC: two animals with TiN site probes, two animals with gold-coated PEDOT site probes. Differences in the behavioural state probably contribute to the variability in event rate. **d**, The event SNR, defined in the Methods. The stability of this signal quality metric suggests that the drop in event rate for PEDOT-1 was due to biological factors unrelated to probe site integrity. **e–g**, Probes (phase 2) of all four shank designs—passive, active, passive switched and active switched—were implanted chronically in the rat mPFC. Recordings were made at least once per week. Data analysis, the implant method and recording procedures are described in detail in the Methods. There is no apparent downward trend in neural activity by either metric (**e**, **f**), thus all four shank technologies can achieve exceptional chronic stability. **g**, mPFC recording, 200 ms of activity traces and examples of waveforms from two sorted units. Inset, dark lines show average waveform overlaid with 30 randomly selected single event waveforms of a neuron located at the top (green) and bottom (red) of the most distal group of 128 sites.



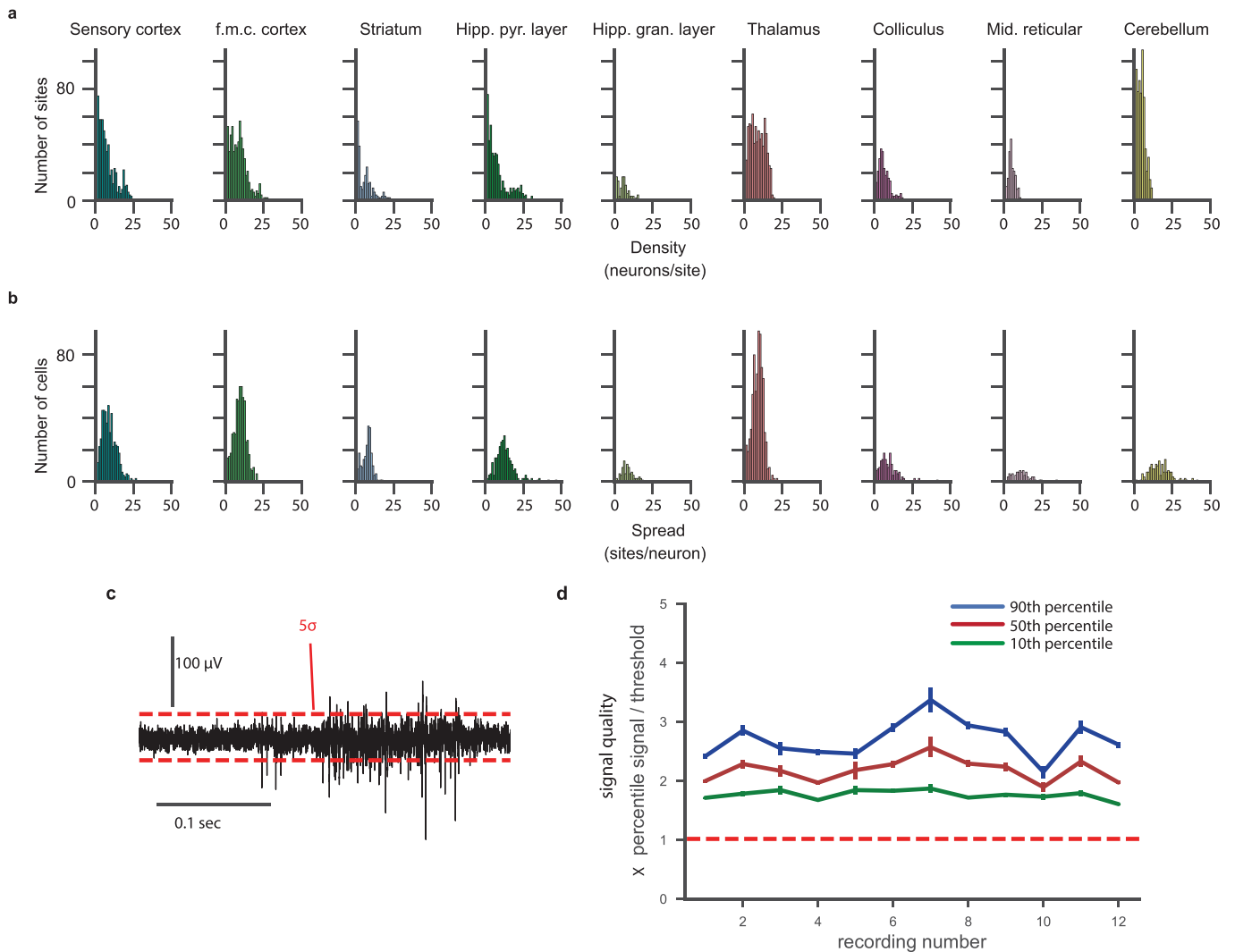
Extended Data Figure 5 | Stability of chronically implanted phase 3 active and switched probe technologies in rats. **a, b**, Phase 3 fully integrated probes: two of four designs were implanted in the mPFC of rats as for phase 2 (Extended Data Fig. 4). One probe with amplified sites and two switchable, unamplified probes (the preferred technology) were implanted. Amplified, switchable probes were implanted but were damaged electronically before adequate recording data could be accumulated. There was no indication of activity loss over the 8 weeks of recording (linear regression *t*-test, one-tailed, $P > 0.1$) except for the top half of one probe (blue). This good performance was expected based on phase 2 results, but the active and active switched probes are 70- μm wide in phase 3 compared to 50- μm wide for phase 2. See Methods for details of data analysis, the implant method and recording procedures. We define an event as time-coincident spikes recorded on a contiguous group of sites for which the maximum amplitude on any site in the group exceeds

the threshold. Across a population of 14 probes chronically implanted in the rat mPFC (phases 2 and 3), we did not observe degradation of spiking activity over 8 weeks (linear regression *t*-test, single-tailed, $P > 0.1$, $n = 30$ sessions). The sole exception to this observation is shown in **a** and **b** above (blue). In this case, the top half of the distal most 3.8 mm array lost nearly all activity over the first 30 days, whereas the bottom ~ 1.9 mm remained stable for the duration of the 8 weeks monitored. A few probe implants became detached from the skull after many months (3 out of 16 implants, 223–482 days after implantation) or surgery wound irritation required the subject animal to be euthanized (but always after at least 20 weeks). **c**, mPFC recording, 200 ms of activity traces and examples of waveforms from two sorted units. Insets, dark lines show the average waveform overlaid with 30 randomly selected single event waveforms of a neuron located at the top (blue) and bottom (red) of the distal most group of 384 sites.



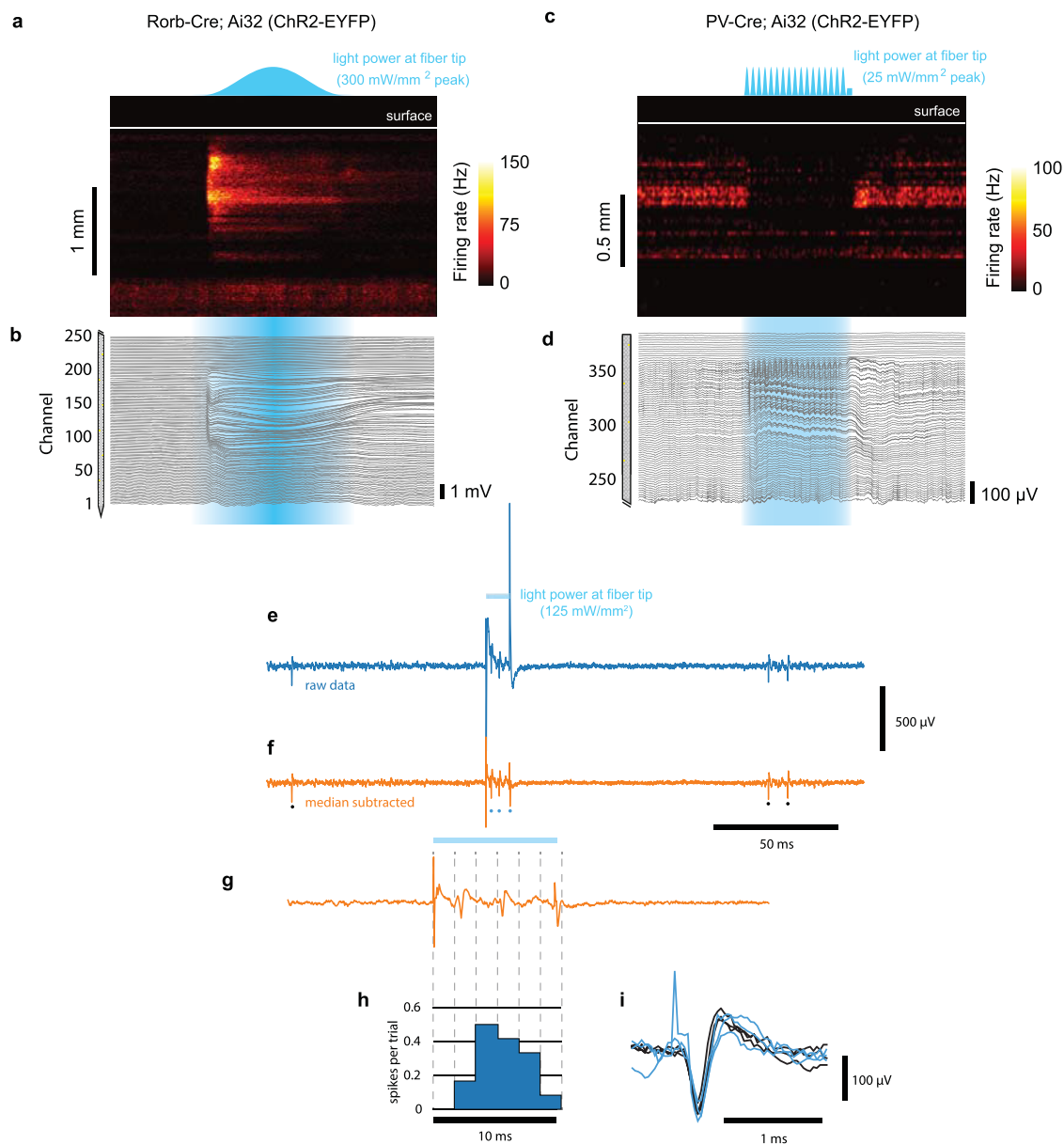
Extended Data Figure 6 | Further examples of LFP data quality. **a**, Two example periods of LFP data, over the entire depth of the probe. The data were filtered with a third-order Butterworth low-pass filter with 300 Hz cut-off frequency, but otherwise unprocessed. Only one channel from each depth along the probe is shown, so the total number of plotted traces is 192 rather than 384. Left example shows an epoch without ripples, and right example shows an epoch with a ripple (indicated by red arrow). The ripple is expanded in the inset. **b**, Quantification of LFP signal amplitude (r.m.s.) across depth. At the right, the anatomical locations of the sections

of the probe are depicted, which were determined from histology, part of which is shown in **c**, along with functional markers such as spike rates and amplitudes. **c**, Histological section depicting the location of the probe (stained with DiI) as it passed through the hippocampus. **d**, Theta-filtered LFP. The same data from **a** (left) were filtered with a third-order bandpass Butterworth filter between 4 and 10 Hz, and are here depicted as a colour map to emphasize the phase inversion at the CA1 pyramidal layer (indicated by the red dashed line).



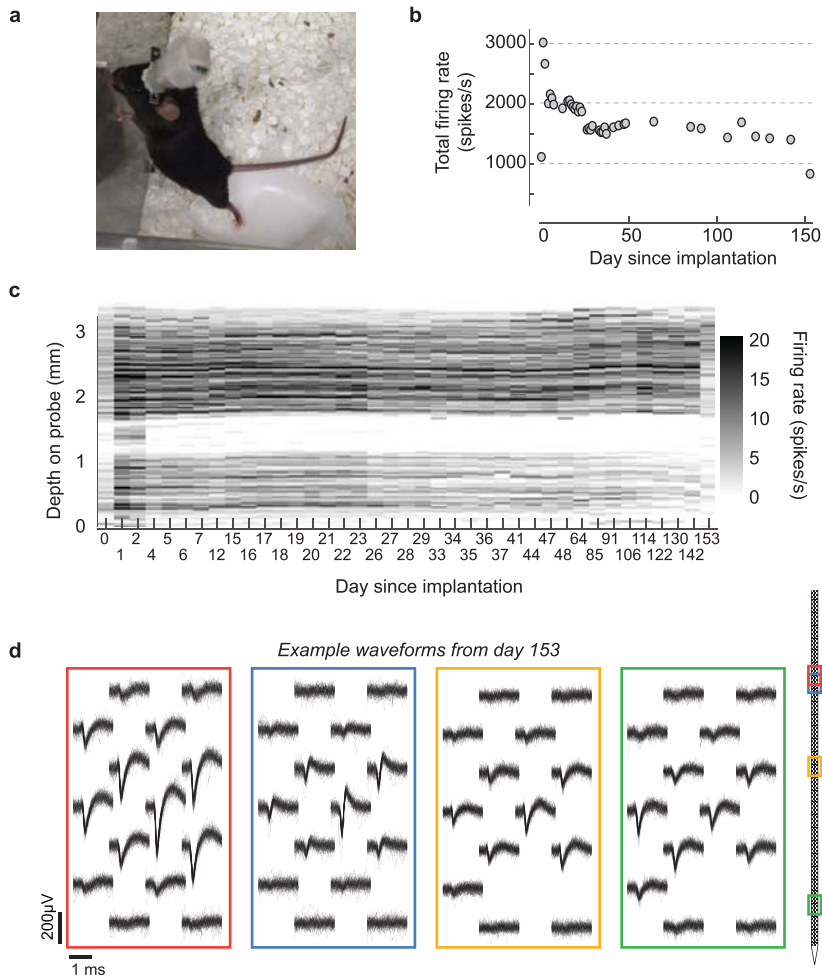
Extended Data Figure 7 | Spike band signal quality across brain areas and multiple acute recordings. **a**, For each channel in each brain area, the number of neurons with a mean waveform greater than $20\ \mu\text{V}$ was counted ('density'). **b**, For each neuron recorded in each brain area, the number of channels on which that neuron produces a mean waveform above $20\ \mu\text{V}$ ('spread') was counted. In a separate set of experiments, the same probe was used for a series of 12 acute *in vivo* recordings in 10 animals

across 4 months. **c**, The signal quality of each recording was computed by measuring the amplitude of detected spikes relative to the detection threshold within a 30 s selection of the recording. The detection threshold used was always 5 times the standard deviation (σ) of the mean signal. **d**, The mean (\pm s.e.m.; $n = 200$) ratio of the ninetieth percentile (blue), fiftieth percentile (red) and tenth percentile (green) to the 5σ detection threshold across all channels with an event, for each recording.



Extended Data Figure 8 | Recording during optogenetic stimulation of excitatory and inhibitory cell populations. **a, b**, A Neuropixels probe was inserted into the primary visual cortex of a Rorb-Cre;Ai32 mouse expressing channelrhodopsin-2 (ChR2) in Rorb-positive cells, which are primarily excitatory neurons of layer 4. Stimulation was carried out with a 465 nm LED coupled to a 200- μ m, 0.66 NA fibre optic cable placed on the surface of the cortex approximately 1 mm from the recording site. Each trial ($n = 20$) consisted of a raised cosine light pulse 1 s in duration, with a peak intensity of 300 mW mm⁻². **a**, Average multiunit firing rate across 250 channels, aligned to the start of the optogenetic stimulus. Location of the brain surface is marked with a white line. **b**, Average LFP band response to the optogenetic stimulus for 125 channels along the left edge of the probe (a subset of the sites in **a**). **c, d**, A Neuropixels probe was inserted into the primary visual cortex of a PV-Cre;Ai32 mouse expressing ChR2 in parvalbumin (PV)-positive cells, which are primarily fast-spiking inhibitory neurons. Stimulation was carried out with a 470 nm laser focused to a \sim 150 μ m diameter spot on the surface of the cortex at the

recording site. Each trial ($n = 15$) consisted of a 500 ms, 40 Hz raised cosine light pulse train, with a peak intensity of 25 mW mm⁻². **c**, Average multiunit firing rate (regular-spiking waveforms only) across 150 channels, aligned to the start of the optogenetic stimulus. Location of the brain surface is marked with a white line. **d**, Average LFP band response to the optogenetic stimulus for 75 channels along the left edge of the probe (a subset of the sites in **c**). **e–i**, Light artefact and detection of optogenetically driven spikes in a PV-Cre;Ai32 mouse. **e**, Raw data for a single trial with optical transients at onset and offset of light stimulation. **f**, The same trial and channel as **e**, after the light-evoked transient was reduced by subtraction of the median of the activity across all channels as in Extended Data Fig. 1. Spike times identified by the spike sorting algorithm are indicated with circles below the trace. **g**, Zoomed-in view of the period of light stimulation. **h**, The average number of spikes, for this unit, during light stimulation. Each bin is 1.7 ms. **i**, Overlaid waveforms for three spikes during light stimulation (blue) and outside of light stimulation (black).



Extended Data Figure 9 | Stability of a probe implanted chronically in a mouse over 21 weeks. **a**, A chronically implanted mouse, 85 days after probe implantation. The subject was a male C57BL/6J mouse, 92 days old at the time of probe implant. The probe is protected by a custom plastic enclosure. Total implant weight was approximately 3.0 g, including the metal headplate (bar with side holes) that was used to fix the head during recordings. **b**, Firing rate across the probe, measured by counting spikes with amplitude $>50 \mu\text{V}$ trough-to-peak at each depth as a function of days since implantation. Day 0 was recorded in the anaesthetized condition during implantation; all subsequent days were recorded during wakefulness. **c**, Total summed firing rate across all channels, showing a decrease in the few days after implantation followed by mostly stable high-yield recordings for a period of 153 days, after which time the experiment was ended by experimenter decision. **d**, Example waveforms from three putative frontal cortical neurons and one neuron in the lateral septal nucleus recorded on day 153 after implantation. Probe icon at the right depicts the location of the waveforms on the probe.

Extended Data Table 1 | Measured operating parameters of the 4 probe types reported (phase 3)

	Option 1	Option 2	Option 3	Option 4
Site Count	384	384	960	966
Channel count	384	384	384	276
Electrode type	Passive	Active	Passive	Active
Shank power (mW)	0	1.31	0	1.31
Base power (mW)		17.5		
Electrode area (μm^2)		144		
Crosstalk (at 1kHz)		< 5%		
Gain		selectable from 50 - 2500		
AP band high-pass corner (kHz)		selectable from 0.3 - 1.0		
AP band low-pass corner (kHz)		10		
LFP band high-pass corner (Hz)		0.5		
LFP band low-pass corner (Hz)		1000		
AP band sampling rate (kHz)		30		
LFP band sampling rate (kHz)		2.5		
AP band noise (μV r.m.s.)	5.7 ± 0.8	6.6 ± 0.8	5.5 ± 0.7	6.6 ± 2.5
LFP band noise (μV r.m.s.)	9.6 ± 5.8	13.0 ± 2.8	8.0 ± 2.5	10.2 ± 1.9

Life Sciences Reporting Summary

Nature Research wishes to improve the reproducibility of the work that we publish. This form is intended for publication with all accepted life science papers and provides structure for consistency and transparency in reporting. Every life science submission will use this form; some list items might not apply to an individual manuscript, but all fields must be completed for clarity.

For further information on the points included in this form, see [Reporting Life Sciences Research](#). For further information on Nature Research policies, including our [data availability policy](#), see [Authors & Referees](#) and the [Editorial Policy Checklist](#).

▶ Experimental design

1. Sample size

Describe how sample size was determined.

Sample sizes for chronic testing probe options were limited by the number of available devices, usually 5 each in two laboratories. Replicated for acute recording were determined when results were consistent within the ability to reproduce the insertion. Physical tests were performed on all available devices. Variation is reflected in the specification in extended data table I.

2. Data exclusions

Describe any data exclusions.

No data were excluded. As described, failed surgeries were not included. A failed surgery was no recorded activity 1 day after implantation.

3. Replication

Describe whether the experimental findings were reliably reproduced.

For device behavior measured on the bench, outstanding reproducibility was obtained, SD of a few percent. For acute recordings, again, little variation is seen. For chronic implants, the limit on the available devices and prevent more replicates than are reported. We see no outliers among the successful experiments, but these numbers are too small to understand expected failure rates for large number of experiments.

4. Randomization

Describe how samples/organisms/participants were allocated into experimental groups.

Devices were sent randomly to researchers without their knowledge of bench test performance data. There is no other blinding, in that individual researchers implanted, recorded and analyzed their own data. Experiments were repeated without collaboration across 2 or 3 locations with similar results in all cases.

5. Blinding

Describe whether the investigators were blinded to group allocation during data collection and/or analysis.

No blinding except in the distribution of devices.

Note: all studies involving animals and/or human research participants must disclose whether blinding and randomization were used.

6. Statistical parameters

For all figures and tables that use statistical methods, confirm that the following items are present in relevant figure legends (or in the Methods section if additional space is needed).

n/a Confirmed

- The exact sample size (n) for each experimental group/condition, given as a discrete number and unit of measurement (animals, litters, cultures, etc.)
- A description of how samples were collected, noting whether measurements were taken from distinct samples or whether the same sample was measured repeatedly
- A statement indicating how many times each experiment was replicated
- The statistical test(s) used and whether they are one- or two-sided (note: only common tests should be described solely by name; more complex techniques should be described in the Methods section)
- A description of any assumptions or corrections, such as an adjustment for multiple comparisons
- The test results (e.g. P values) given as exact values whenever possible and with confidence intervals noted
- A clear description of statistics including central tendency (e.g. median, mean) and variation (e.g. standard deviation, interquartile range)
- Clearly defined error bars

See the web collection on [statistics for biologists](#) for further resources and guidance.

► Software

Policy information about [availability of computer code](#)

7. Software

Describe the software used to analyze the data in this study.

The spike sorting software is already public domain, JRClust or kilosort. We expect that both packages will remain public domain resources for the foreseeable future.

For manuscripts utilizing custom algorithms or software that are central to the paper but not yet described in the published literature, software must be made available to editors and reviewers upon request. We strongly encourage code deposition in a community repository (e.g. GitHub). [Nature Methods guidance for providing algorithms and software for publication](#) provides further information on this topic.

► Materials and reagents

Policy information about [availability of materials](#)

8. Materials availability

Indicate whether there are restrictions on availability of unique materials or if these materials are only available for distribution by a for-profit company.

The primary materials, probes, are not yet available for wide distribution. We plan to "sell" these devices beginning next year through both for profit and nonprofit channels.

9. Antibodies

Describe the antibodies used and how they were validated for use in the system under study (i.e. assay and species).

Commercially purchased and not tested.

10. Eukaryotic cell lines

a. State the source of each eukaryotic cell line used.

None used

b. Describe the method of cell line authentication used.

NA

c. Report whether the cell lines were tested for mycoplasma contamination.

NA

d. If any of the cell lines used are listed in the database of commonly misidentified cell lines maintained by [ICLAC](#), provide a scientific rationale for their use.

NA

► Animals and human research participants

Policy information about [studies involving animals](#); when reporting animal research, follow the [ARRIVE guidelines](#)

11. Description of research animals

Provide details on animals and/or animal-derived materials used in the study.

Rodents used in these studies are described in the text and supplemental information. They are all unmodified commercial strains.

12. Description of human research participants

Describe the covariate-relevant population characteristics of the human research participants.

NA